PII S0016-7037(99)00425-1

Trace element partitioning between coexisting biotite and muscovite from metamorphic rocks, Western Labrador: Structural, compositional and thermal controls

Panseok Yang and Toby Rivers*

Department of Earth Sciences, Memorial University of Newfoundland, St. John's, NF, Canada A1B 3X5

Abstract—Coexisting biotite and muscovite in ten metapelitic and quartzofeldspathic rocks from western Labrador have been analyzed by electron microprobe for major and minor elements and by a laser ablation microprobe coupled to ICP-MS (LAM-ICP-MS) for selected trace elements—Li, Sc, V, Cr, Mn, Co, Ni, Cu, Zn, Rb, Sr, Y, Zr, Nb, Cs, Ba, REE, Hf and Ta. The samples have experienced a single prograde Grenvillian metamorphism ranging from 490 to 680°C and from 7 to 12 kbar. The trace element compositions of coexisting micas in the metamorphic rocks are used to assess the effects of crystal structure, major element composition and temperature on the partitioning of each element between biotite and muscovite.

Overall, trace element distributions are systematic across the range of metamorphic grade and bulk composition, suggesting that chemical equilibrium was approached. Most distribution coefficients (biotite/muscovite) show good agreement with published data. However, distribution coefficients for Co and Sr are significantly different from previous determinations, probably because of contamination associated with older data obtained by bulk analysis techniques. The sequence of distribution coefficients is governed mainly by the ionic radii and charges of substituting cations compared to the optimum ionic radius of each crystallographic site in the micas. In particular, distribution coefficients exhibit the sequence Cr^{3+} (0.615 Å) $> V^{3+}$ (0.64 Å) $> Sc^{3+}$ (0.745 Å) in VI-sites, and Ba^{2+} (1.61 Å) $> Sr^{2+}$ (1.44 Å) and Cs^+ (1.88 Å) $> K^+$ (1.64 Å) $> Rb^+$ (1.72 Å) $> Na^+$ (1.39 Å) in XII-sites. The distributions of Li, Sc, Sr and Ba appear to be thermally sensitive but are also controlled by major element compositions of micas. V and Zr partitioning is dependent on T and may be used to cross-check thermometry calculations where the latter suffer from retrograde re-equilibration and/or high concentrations of Fe^{3+}. The ranges and dependence of distribution coefficients on major element compositions provide important constraints on the values that can be used in geochemical modeling. *Copyright © 2000 Elsevier Science Ltd*

1. INTRODUCTION

Major element partitioning between coexisting phases is an important aspect of the characterization of phase equilibrium relationships as a function of pressure (P), temperature (T) and compositional variables (X) and is the basis for classical geothermobarometry (Kretz, 1961). In principle, the concept should also extend to trace element partitioning which should therefore also be useful to estimate P-T conditions during metamorphism (e.g., Heinrich et al., 1997; Bea et al., 1997). In addition to thermobarometry, studies of the partitioning of trace elements among coexisting metamorphic minerals can provide valuable information about equilibrium and petrogenesis (e.g., Haack et al., 1984; Dahl et al., 1993; Hickmott et al., 1987; Hickmott and Spear, 1992; Johnson, 1994; Kretz et al., 1999; Yang et al., 1999). However, the subject has been relatively little investigated because of the difficulty in obtaining uncontaminated trace element analyses and due to complications resulting from crystal chemistry and the composition of host minerals.

Micas are petrogenetically very useful minerals because of their high abundance in many metamorphic rocks, their wide range of stability, their relatively simple mineralogy and their potential to provide information about P-T conditions. To extract meaningful petrogenetic information, accurate measure-

ment of the trace element partition coefficients for a wide range of trace elements in various metamorphic environments is essential. At present, there are relatively few published trace element partitioning studies for biotite-muscovite pairs in metamorphic systems (Butler, 1967; Moorbath et al., 1968; Dutrow et al., 1986; Shearer et al., 1986; Hervig and Peacock, 1989; Dahl et al., 1993; Domanik et al., 1993). Moreover, very little is known about the dependence of the biotite/muscovite distribution coefficients on the intensive and extensive variables, constraining geochemists to adopt a largely empirical approach using constant average distribution values in their modeling (e.g., Haack et al., 1984; Johnson, 1994). In addition, most trace element data in the earlier publications were obtained from bulk analyses of mineral separates, which have commonly proved to be contaminated with micro-inclusions of accessory minerals (Michael, 1988). The use of mineral separates also does not take mineral zoning into account, so the results may not yield equilibrium partition coefficients. These problems are especially acute in medium grade metamorphic rocks where micro-inclusions are ubiquitous. In this study, we have determined partition coefficients for selected trace elements in coexisting biotite and muscovite from ten metapelitic and quartzofeldspathic rocks from western Labrador using a microbeam technique and have examined the variation of biotite/muscovite partition coefficients as a function of crystal structure, variations in major element composition and metamorphic temperature.

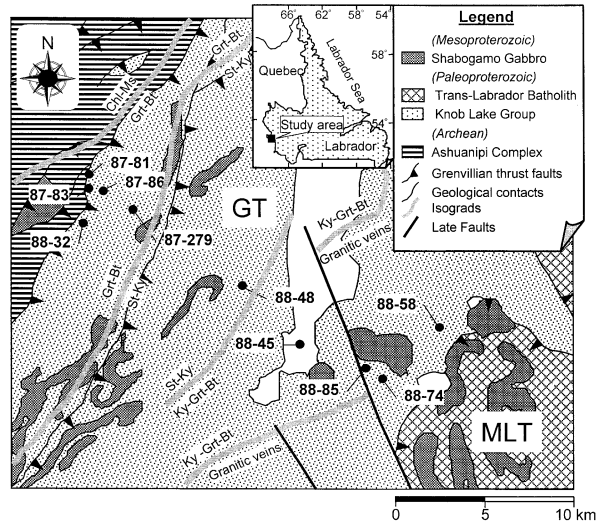*Author to whom correspondence should be addressed.

Fig. 1. Generalized geologic map of the northern Grenville province in western Labrador, Canada, showing metamorphic isograds and locations of the ten analyzed samples. GT-Gagnon terrane; MLT-Molson Lake terrane Geologic map from Connelly et al. (1996) and metamorphic isograds from Rivers (1983b) and van Gool (1992).

2. GEOLOGY AND SAMPLES

The ten analyzed samples come from Gagnon terrane in the Grenville Province of western Labrador (Fig. 1). Gagnon terrane comprises a metamorphic foreland fold-and-thrust belt (Rivers, 1983a,b; van Gool, 1992), that is separated from the Superior Province foreland in the northwest by the Grenville Front, and is tectonically overlain by Molson Lake terrane to the southeast. Metasediments in Gagnon terrane, which are part of the Paleoproterozoic Knob Lake Group, were deposited on the passive continental margin of the Superior Craton and experienced a single Barrovian-type regional metamorphism during the Grenvillian Orogeny at ca. 1000 Ma (Rivers, 1983b; Brown et al., 1992; van Gool,1992; Rivers et al., 1993; Schwarz, 1998). During this orogenic event, Gagnon terrane was overthrust by Molson Lake terrane, composed of Late Paleoproterozoic to Mesoproterozoic granitoid and gabbroic rocks, and incorporated into the base of a major thrust wedge.

Metamorphic grade increases from greenschist facies in the northwest, at the Grenville Front, to upper amphibolite facies in the southeast, near Molson Lake terrane. Six metamorphic zones have been outlined by Rivers (1983b) based on the diagnostic mineral assemblages: chlorite-muscovite (I), biotite-muscovite (II), garnet-biotite (III), staurolite-kyanite (IV), biotite-kyanite-garnet (V) and biotite-kyanite-garnet-granitic veins (VI) in order of increasing metamorphic grade (Fig. 1). The isograds were telescoped during thrusting (van Gool, 1992), and the apparent absence of a staurolite-biotite zone between the garnet-biotite and staurolite-kyanite zones may be due either to telescoping and/or to poor exposure. The samples chosen for this study include five from the garnet-biotite zone (referred to as low-T samples) and another five from staurolite-kyanite, biotite-kyanite-garnet and biotite-kyanite-garnet-granitic veins zones (referred to as high-T samples). Micas from the lowest grade zone are very fine grained, presenting difficulties for the LAM-ICP-MS technique, and were not included in this study.

All selected rocks are foliated and are composed principally of quartz (26–62% modal), micas (35–54% modal) and lesser amounts of garnet, kyanite, chlorite, epidote and plagioclase, with accessory minerals constituting the remainder (Table 1). All of the samples have at least one Ti-saturating phases such as ilmenite and rutile in the matrix. Plagioclase occurs in all samples except 88–58. Accessory minerals in the samples include pyrite, ilmenite, rutile, monazite, apatite, tourmaline, graphite and zircon. Both biotite and muscovite show little sign of retrogression and secondary muscovite rarely occurs in these rocks. Inclusions of apatite, zircon and ilmenite are common in the biotite crystals, and, to a lesser extent, in the white mica. A marked coarsening of the grain size of the micas occurs within the staurolite-kyanite zone and coincides with the disappearance of primary chlorite from the assemblage (Table 1). Mineral assemblages, textures and reactions in metapelitic rocks of the Gagnon terrane in western Labrador are described in detail elsewhere (e.g., Rivers, 1983b; van Gool, 1992).

3. ANALYTICAL METHODS

3.1. Electron Microprobe Analysis

Major and minor element analyses were performed using the Cameca® SX-50 electron microprobe at Memorial University

Table 1. Mineral assemblages and modal percentages of the ten metapelitic samples from western Labrador.

Sample	Zones	Qtz	Ms	Bt	Chl	Ep	Pl	Ky	Grt	Tur	Ap	Rt	Zrn	Ilm	Py	Mo	Gr
87-81	III	41	28	26			<1		<1	<1	<1	<1	<1	<1	<1		
87-83	III	53	11	28	<1	<1[a]	<1		4	<1	<1		<1	<1			<1
87-86	III	40	11	43	<1	<1[a]	<1		<1	<1	<1		<1	<1			<1
87-279	III	48	16	23	4[b]	<1	<1		3		<1	<1	<1	<1	<1		<1
88-32	III	30	19	35	<1	<1[a]	<1		10	<1	<1		<1	<1			
88-48	IV	26	10	44	4[b]		<1	2	10	<1		<1	<1	<1[a]	<1		
88-45	V	44	27	11			<1	<1	11			<1	<1		<1	<1	
88-85	V	62	29	6			<1	2	<1		<1	<1	<1	<1	<1	<1[a]	
88-74	VI	34	26	23			5	9	<1	<1	<1	<1[a]	<1	<1	<1	<1	
88-58	VI	34	43	8				11			<1	<1	<1	<1		<1	

[a] Minerals occur only as inclusions in garnet.
[b] Secondary minerals. Characteristic mineral assemblages of metamorphic zones are: III; Grt-Bt, IV; St-Ky; V; Bt-Ky-Grt and VI; Bt-Ky-Grt granitic veins. Mineral abbreviations after Kretz (1983).

Table 2. Precision and mean values for a glass standard BCR-2 determined by LAM-ICP-MS.

Elements	AVG	STD	RSD	DL	No	Known	AVG/Known
Li	8.4			5.955	1	9.98	0.84
Sc	31.4	0.8	2%	0.653	5	32.6	0.96
TiO_2	2.05	0.04	2%	1.6E-4	10	2.24	0.91
V	402	11	3%	0.068	7	407	0.99
Cr	15.0	2.5	16%	2.501	6	16	0.94
MnO	0.18	0.01	4%	5.1E-5	7	0.177	1.03
Co	36.4	1.7	5%	0.325	7	37	0.98
Ni	11.3	1.4	12%	1.041	7	13	0.87
Cu	20.5	1.0	5%	0.356	5	19	1.08
Zn	173	12	7%	0.581	5	129.5	1.33
Rb	54			0.018	2	47.51	1.14
Sr	337.2	7.6	2%	0.006	5	337	1.00
Y	31.9	1.7	5%	0.007	7	32.51	0.98
Zr	170.5	6.3	4%	0.021	10	184.4	0.92
Nb	10.8	1.0	9%	0.006	5	13.14	0.82
Cs	1.3			0.014	2	1.19	1.09
Ba	644	21	3%	0.035	10	681	0.95
La	25.5	1.1	4%	0.005	7	25.3	1.01
Ce	54.3	1.7	3%	0.003	9	53.6	1.01
Hf	4.8	0.3	5%	0.021	7	5.17	0.94
Ta	0.6	0.1	9%	0.004	7	0.78	0.77

Based on 10 determinations over the period March 19, 1996 to April 5, 1997. AVG = average; STD = standard deviation; RSD = relative standard deviation; DL = detection limits; No = number of observations; and Known = literature values from Govindaraju (1994).

of Newfoundland using energy dispersive (ED) and wavelength dispersive (WD) methods simultaneously. Analyses were carried out using a 15 kV accelerating voltage, 10 nA current and a 5 micron beam diameter. ED analyses used a cobalt gain calibration. Ti, F and Cl were determined by WD analysis using ilmenite, apatite and tugtupite ($Na_4AlBeSi_4O_{12}Cl$) as standards, respectively. Analyses were obtained on three or more crystals of biotite and muscovite in each of the ten samples. Precision at the 1σ level for Ti (used for calibration of ICP-MS results, see below) was better than 6% relative in both biotite and muscovite.

3.2. LAM-ICP-MS Analysis

Trace element compositions in micas were determined by a laser ablation system coupled to an ICP-MS (Fisons VG PQII +S®) at Memorial University of Newfoundland. The LAM system incorporates a Nd:YAG laser (266 nm wavelength), a custom built sample cell and an Ar carrier gas system. Details of the system are described in Jackson et al. (1992), Jenner et al. (1994) and Taylor et al. (1997).

Data acquisition was performed by peak jumping in pulse counting mode, acquiring individual intensity data for each analyte isotope during each mass spectrometer sweep (~1 sec). A total of about 480 sweeps, comprising a gas background interval of about 200 sweeps followed by an ablation interval of about 280 sweeps was performed for each analysis. Calibration was conducted on the NIST SRM-610 glass standard, and BCR-2 was used to check the data quality during each run. Ti was routinely employed as the internal standard, based on electron microprobe measurement of the TiO_2 contents in the micas.

Data reduction followed the protocol outlined by Longerich et al. (1996). Limit of detection for BCR-2 for a ~50 μm beam size and ~0.5 mJ/pulse was typically in the range 3–35 ppb for most high-mass elements (Rb to Ta), and between 68 and 6000 ppb for lower-mass elements (Li to Zn) (Table 2). However, detection limits for samples are different from the glass standard because of different beam diameters, counting times and ablation energy used for each single analysis. For high-T micas, we used a ~70 μm beam size and ~0.7 mJ/pulse of laser energy. For low-T micas, we had to reduce the beam size and pulse energy by almost half because of their smaller size. According to Longerich et al. (1996), the difference in beam size between low- and high-T micas results in at least a fourfold increase in the detection limit.

Repeated measurements of BCR-2 glass at the same ablation conditions yielded a precision (1σ) of better than 5 and 10% relative for absolute concentrations above and below 1 ppm, respectively, except for Cr and Ni. The poor precision obtained for Cr and Ni is attributed to their concentrations approaching detection limits in the glass. Zn analyses clearly show the effects of fractionation during the laser ablation, as indicated by increasing signals over time, invariably resulting in higher concentrations compared to the literature values (Table 2). Because of the fractionation effect observed, the lowest measured value of Zn for each sample was used.

The time-resolved analysis of the LAM allows detection of zoning and inclusions in the analyzed mineral grain during ablation, which is a great advantage over other microbeam techniques such as PIXE and SIMS. However, the presence of sub-microscopic inclusions below the resolution of the time-resolved signal (a few microns) cannot be ruled out. Indeed, Zr, La and Ce analyses of micas are highly variable on a thin-section scale. Since micro-inclusion phases enriched in Zr, La and Ce, such as zircon, monazite and apatite, were found in the analyzed micas, we consider the most reliable data to be those with the lowest concentrations of these elements. Zn, Zr, La and Ce data therefore should be considered as only semi-quantitative.

Electron microprobe and LAM-ICP-MS analyses of biotite

Table 3. Averages and standard deviations (1σ) of biotite analyses.

	87-81F	87-81I	87-81K	87-83C	87-83D	87-86F	88-32A	88-32B	87-279D	87-279F	87-279G
(wt.%)											
SiO$_2$	36.93 (0.16)	36.93 (0.16)	36.93 (0.16)	36.98 (0.18)	36.98 (0.18)	37.23 (0.26)	35.92 (0.38)	35.92 (0.38)	37.16 (0.62)	37.16 (0.62)	37.16 (0.62)
TiO$_2$	1.56 (0.05)	1.56 (0.05)	1.56 (0.05)	1.57 (0.02)	1.57 (0.02)	1.62 (0.07)	1.54 (0.08)	1.54 (0.08)	1.65 (0.06)	1.65 (0.06)	1.65 (0.06)
Al$_2$O$_3$	17.35 (0.16)	17.35 (0.16)	17.35 (0.16)	17.67 (0.10)	17.67 (0.10)	17.75 (0.19)	17.58 (0.27)	17.58 (0.27)	17.64 (0.33)	17.64 (0.33)	17.64 (0.33)
FeO$^{\#}$	19.92 (0.27)	19.92 (0.27)	19.92 (0.27)	19.57 (0.32)	19.57 (0.32)	19.23 (0.26)	21.91 (0.27)	21.91 (0.27)	17.93 (0.08)	17.93 (0.08)	17.93 (0.08)
MgO	10.08 (0.18)	10.08 (0.18)	10.08 (0.18)	10.58 (0.14)	10.58 (0.14)	10.74 (0.13)	8.97 (0.14)	8.97 (0.14)	11.25 (0.19)	11.25 (0.19)	11.25 (0.19)
Na$_2$O	D.L.	D.L.	D.L.	0.35	0.35	D.L.	D.L.	D.L.	D.L.	D.L.	D.L.
K$_2$O	9.26 (0.20)	9.26 (0.20)	9.26 (0.20)	9.61 (0.10)	9.61 (0.10)	9.64 (0.15)	9.240 (0.23)	9.24 (0.23)	9.94 (0.16)	9.94 (0.16)	9.94 (0.16)
F	0.363 (0.042)	0.363 (0.042)	0.363 (0.042)	0.510 (0.050)	0.510 (0.050)	0.540 (0.071)	0.500 (0.009)	0.500 (0.009)	0.590 (0.025)	0.590 (0.025)	0.590 (0.025)
Cl	0.138 (0.025)	0.138 (0.025)	0.138 (0.025)	0.058 (0.010)	0.058 (0.010)	0.061 (0.013)	0.108 (0.011)	0.108 (0.011)	0.069 (0.007)	0.069 (0.007)	0.069 (0.007)
Total	95.43	95.43	95.43	96.68	96.68	96.56	95.53	95.53	95.97	95.97	95.97
(ppm)											
Li		103	101 (19)	132 (13)	99 (16)	168	91 (5)		125	123 (12)	127
Ca	D.L.	321	415 (128)	D.L.	275 (98)	323	244 (48)	D.L.	D.L.	272	D.L.
Sc	18.5	15.4	12.9 (0.9)	11.7 (0.8)	12.8 (1.3)	17.2	11.7 (1.4)	12.9	14.4	20.3 (2.5)	22.2 (3.0)
V	191	153	146 (2)	140 (15)	139 (2)	141	181 (10)	192	655	665 (102)	653 (65)
Cr	173	198	180	89	94 (3)	106	89 (8)	86	198	172 (14)	183
Mn	1541	1487	1325 (48)	974 (123)	957 (20)	948	530 (30)	539	1360	1050 (162)	986
Co	50	45	40 (5)	47 (7)	48 (6)	49	39 (3)	40	20	17 (3)	21 (4)
Ni	91	90	86 (16)	161 (14)	149 (6)	108	67 (8)	69	39	48 (4)	63 (10)
Cu	8.36	5.92	12.50	5.75 (2.04)	6.50 (0.55)	D.L.	4.51 (0.49)	D.L.	D.L.	5.64 (0.28)	5.50
Zn*	174	174	174	323	323	281	79	79	212	212	212
Rb		396	448 (15)		549 (29)	401	409 (40)			322 (35)	416 (73)
Sr	1.9	2.1	1.7 (0.5)	1.0 (0.1)	1.2 (0.1)	1.2	2.5 (0.4)	D.L.	2.0	1.5 (0.1)	1.9 (0.4)
Y*	0.17	0.17	0.17	0.25	0.25	0.27	0.14	0.14	0.15	0.15	0.15
Zr*	0.10	0.10	0.10	D.L.	D.L.	D.L.	0.08	0.08	0.10	0.10	0.10
Nb	47.8	53.6	55.9 (1.6)	38.3 (2.7)	58.5 (3.1)	45.8	39.1 (2.2)	D.L.	35.3	34.2 (7.1)	35.2
Cs		18.8	19.7 (0.4)		30.5 (3.5)	19.1	9.6 (1.3)			17.1 (2.4)	17.3
Ba	1193	1278	1282	1037 (162)	1190 (42)	873	1002 (38)	1275	1074	912 (97)	1118 (265)
La*	0.2	0.2	0.2	0.4	0.4	D.L.	0.1	0.1	0.5	0.5	0.5
Ce*	0.6	0.6	0.6	0.4	0.4	D.L.	0.2	0.2	1.0	1.0	1.0
Hf	D.L.	0.11	D.L.	D.L.	D.L.	0.07	0.06 (0.03)	D.L.	D.L.	0.05	D.L.
Ta	D.L.	3.766	3.839 (0.079)	3.063 (0.400)	4.004 (0.026)	2.935	0.946 (0.048)	D.L.	2.414	1.466 (0.261)	1.076

Table 3. (Continued)

	88-48C	88-45D	88-45E	88-74C	88-74D	88-74E	88-85C	88-85D	88-58A	88-58B	88-58C
(wt.%)											
SiO_2	37.81 (0.37)	37.58 (0.56)	37.58 (0.56)	37.08 (0.09)	37.08 (0.09)	37.08 (0.09)	37.40 (0.31)	37.40 (0.31)	36.38 (0.31)	36.38 (0.31)	36.38 (0.31)
TiO_2	1.21 (0.05)	1.68 (0.08)	1.68 (0.08)	2.12 (0.08)	2.12 (0.08)	2.12 (0.08)	1.71 (0.09)	1.71 (0.09)	2.13 (0.21)	2.13 (0.21)	2.13 (0.21)
Al_2O_3	19.09 (0.18)	18.58 (0.33)	18.58 (0.33)	18.34 (0.15)	18.34 (0.15)	18.34 (0.15)	18.92 (0.33)	18.92 (0.33)	18.01 (0.08)	18.01 (0.08)	18.01 (0.08)
$FeO^{\#}$	14.57 (0.34)	16.27 (0.30)	16.27 (0.30)	17.27 (0.12)	17.27 (0.12)	17.27 (0.12)	16.40 (0.48)	16.40 (0.48)	20.87 (0.67)	20.87 (0.67)	20.87 (0.67)
MgO	13.89 (0.25)	12.01 (0.46)	12.01 (0.46)	11.83 (0.15)	11.83 (0.15)	11.83 (0.15)	12.49 (0.25)	12.49 (0.25)	9.54 (0.36)	9.54 (0.36)	9.54 (0.36)
Na_2O	0.48 (0.05)	0.41	0.41	0.54 (0.11)	0.54 (0.11)	0.54 (0.11)	0.41 (0.01)	0.41 (0.01)	0.40	0.40	0.40
K_2O	9.45 (0.07)	7.70 (0.19)	7.70 (0.19)	9.29 (0.15)	9.29 (0.15)	9.29 (0.15)	8.50 (0.09)	8.50 (0.09)	9.73 (0.16)	9.73 (0.16)	9.73 (0.16)
F	0.261 (0.024)	0.374 (0.070)	0.374 (0.070)	0.214 (0.010)	0.214 (0.010)	0.214 (0.010)	0.435 (0.062)	0.435 (0.062)	0.349 (0.027)	0.349 (0.027)	0.349 (0.027)
Cl	0.024 (0.003)	D.L.	D.L.	D.L.	D.L.	D.L.	0.010	0.010	0.032 (0.013)	0.032 (0.013)	0.032 (0.013)
Total	96.68	94.45	94.45	96.59	96.59	96.59	96.09	96.09	97.29	97.29	97.29
(ppm)											
Li		315 (25)	305 (21)	198 (70)	222 (1)	206	346 (15)	313	186	193	
Ca	D.L.	293	301 (93)	233 (38)	218 (25)	254	234 (43)	243 (95)	295	209	D.L.
Sc	10.9 (1.2)	5.4 (0.5)	6.3 (0.6)	14.7 (1.2)	14.1 (0.9)	12.5	4.8 (0.1)	5.1 (0.3)	12.8	12.6 (1.8)	11.9 (1.6)
V	151 (20)	219 (29)	230 (18)	251 (8)	246 (14)	260 (15)	256 (4)	261 (18)	131	114 (6)	104 (11)
Cr	D.L.	379	343 (4)	338 (37)	328 (42)	296 (49)	345 (29)	366 (42)	174	194 (21)	172
Mn	31 (3)	34 (2)	39 (4)	227 (22)	229 (18)	216 (8)	42 (2)	44 (5)	156	160 (20)	164 (30)
Co	49 (4)	26 (2)	26 (1)	112 (9)	110 (10)	107 (10)	31 (2)	35 (4)	52	43 (4)	39 (5)
Ni	97 (21)	62 (3)	59 (9)	279 (13)	258 (18)	276 (17)	46 (7)	46 (8)	108	103 (13)	107 (18)
Cu	3.57 (0.25)	7.11 (1.16)	10.44 (4.40)	6.68 (0.25)	5.86 (0.05)	6.50	7.43 (0.98)	6.65	5.77	4.98 (0.04)	5.32 (0.86)
Zn*	77	570	570	251	251	251	408	408	475	475	475
Rb		673	705	527 (2)	459 (9)	479	669 (18)	611	456	380	
Sr	2.0 (0.2)	2.4 (0.2)	1.9 (0.2)	1.9 (0.3)	2.5 (0.3)	1.8 (0.3)	4.7 (0.3)	5.4 (0.5)	4.8	5.4 (1.1)	3.8 (0.4)
Y*	D.L.	0.08	0.08	D.L.	D.L.	D.L.	0.07	0.07	0.04	0.04	0.04
Zr*	0.12	0.15	0.15	0.11	0.11	0.11	0.14	0.14	0.15	0.15	0.15
Nb	21.7 (3.5)	0.9 (0.2)	0.8	18.2 (1.1)	18.5 (0.5)	17.7 (1.4)	1.1 (0.3)	1.4 (0.4)	24.1	25.8	D.L.
Cs		36.4	40.4	9.9 (0.3)	8.3 (0.5)	8.4	31.2 (4.5)	38.0 (7.4)	26.8	25.8	
Ba	409 (27)	810 (25)	680 (38)	576 (57)	605 (59)	615 (37)	1095 (72)	1203 (208)	396	401 (14)	366 (42)
La*	0.6	0.1	0.1	0.0	0.0	0.0	0.1	0.1	0.2	0.2	0.2
Ce*	1.0	0.3	0.3	0.0	0.0	0.0	0.2	0.2	0.2	0.2	0.2
Hf	0.02	0.05	0.02	0.01	0.01	0.02 (0.01)	0.08 (0.01)	0.08 (0.02)	D.L.	D.L.	D.L.
Ta	0.855 (0.097)	0.048 (0.012)	0.030 (0.014)	1.048 (0.124)	1.020 (0.100)	1.011 (0.150)	0.076 (0.003)	0.076 (0.009)	2.449	3.084	D.L.

Notes: # Total Fe as FeO. * For these elements the lowest value within a sample is reported because of fractionation during laser ablation (Zn) and contamination from micro-inclusions (Y, Zr and REE). D.L. and blank represent data below detection limits and elements not determined, respectively. Italicized elements are present in concentrations lower than 3 times detection limits in most analyses. Values in parentheses are standard deviations at 1σ level.

Table 4. Averages and standard deviations (1σ) of muscovite analyses.

	87-81F	87-81I	87-81K	87-83C	87-83D	87-86F	88-32A	88-32B	87-279D	87-279F	87-279G
(wt.%)											
SiO_2	47.02 (0.40)	47.02 (0.40)	47.02 (0.40)	46.47 (0.07)	46.47 (0.07)	47.17 (0.32)	46.83 (0.18)	46.83 (0.18)	46.92 (0.19)	46.92 (0.19)	46.92 (0.19)
TiO_2	0.39 (0.01)	0.39 (0.01)	0.39 (0.01)	0.38 (0.04)	0.38 (0.04)	0.45 (0.03)	0.37 (0.02)	0.37 (0.02)	0.74 (0.05)	0.74 (0.05)	0.74 (0.05)
Al_2O_3	34.44 (0.30)	34.44 (0.30)	34.44 (0.30)	34.14 (1.04)	34.14 (1.04)	33.85 (0.43)	33.87 (0.72)	33.87 (0.72)	33.53 (0.26)	33.53 (0.26)	33.53 (0.26)
$FeO^{\#}$	1.76 (0.09)	1.76 (0.09)	1.76 (0.09)	1.67 (0.32)	1.67 (0.32)	1.79 (0.17)	2.10 (0.17)	2.10 (0.17)	1.59 (0.09)	1.59 (0.09)	1.59 (0.09)
MgO	1.09 (0.15)	1.09 (0.15)	1.09 (0.15)	1.14 (0.27)	1.14 (0.27)	1.26 (0.07)	1.16 (0.06)	1.16 (0.06)	1.29 (0.05)	1.29 (0.05)	1.29 (0.05)
Na_2O	0.88 (0.33)	0.88 (0.33)	0.88 (0.33)	0.96 (0.32)	0.96 (0.32)	0.89 (0.17)	0.66 (0.20)	0.66 (0.20)	0.90 (0.04)	0.90 (0.04)	0.90 (0.04)
K_2O	10.07 (0.32)	10.07 (0.32)	10.07 (0.32)	10.05 (0.43)	10.05 (0.43)	10.14 (0.22)	10.71 (0.24)	10.71 (0.24)	10.19 (0.08)	10.19 (0.08)	10.19 (0.08)
F	0.090 (0.003)	0.090 (0.003)	0.090 (0.003)	0.145 (0.046)	0.145 (0.046)	0.126 (0.021)	0.113 (0.009)	0.113 (0.009)	0.112 (0.029)	0.112 (0.029)	0.112 (0.029)
Cl	D.L.	D.L.	D.L.	D.L.	D.L.	0.031	D.L.	D.L.	D.L.	D.L.	D.L.
Total	95.70	95.70	95.70	94.91	94.91	95.65	95.79	95.79	95.22	95.22	95.22
(ppm)											
Li	D.L.	66 (7)	71	54	54 (2)	91	17 (1)	D.L.		52 (14)	56
Ca	D.L.	710	D.L.	D.L.	D.L.	775	716 (132)	D.L.	D.L.	1055 (523)	571
Sc	53.0 (4.2)	45.8 (5.9)	38.4 (2.6)	31.7	52.3 (0.7)	53.3	47.3 (6.7)	44.2 (12.7)	54.9	66.5 (12.2)	74.4 (13.7)
V	289 (14)	346	301 (66)	312	293 (11)	309	372 (30)	350 (25)	1364	1336 (173)	1259 (283)
Cr	D.L.	D.L.	155 (4)	143	145	67	103 (19)	D.L.	D.L.	240	179 (32)
Mn	51.4	76.7	41.0	41.1	58.1 (20.4)	48.4	30.6 (8.9)	28.7 (4.3)	75.5	62.9 (1.5)	67.8 (19.9)
Co	3.07	3.69 (0.19)	3.31	D.L.	4.67 (0.29)	3.54	2.26 (0.03)	D.L.	D.L.	1.51 (0.68)	1.93 (0.85)
Ni	D.L.	11.81	D.L.	11.29	13.93 (0.63)	8.03	3.68 (0.16)			5.80 (3.50)	5.02
Cu	3.39	3.47 (2.13)		D.L.	2.49	1.21	1.33 (0.29)			4.36 (3.10)	3.43 (4.56)
Zn*	13	13	13	22	22	28	9	9	16	16	16
Rb	127	239 (32)		151	290 (1)	244	232 (17)		178	204 (40)	185 (38)
Sr		149 (5)			204 (20)	161	333 (64)	D.L.		138 (14)	131 (19)
Y*	0.33	0.33	0.33	0.28	0.28	0.17	0.27	0.27	0.09	0.09	0.09
Zr*	0.12	0.12	0.12	0.53	0.53	0.19	0.17	0.17	0.23	0.23	0.23
Nb	25.2 (3.9)	D.L.	27.2 (1.4)	26.2	40.5 (1.6)	28.0	25.4 (1.9)	D.L.		22.4 (18.6)	19.4 (20.7)
Cs		1.18 (0.16)	0.74 (0.14)		2.10 (0.17)	1.41	0.83 (0.02)			1.53 (0.47)	1.69 (0.30)
Ba	5712 (382)	7201 (250)	5842	3900	6176 (447)	4935	4367 (572)	4747 (364)	4216	4014 (512)	3938 (702)
La*	D.L.	D.L.	D.L.	D.L.	D.L.	0.028	0.057	0.057	0.042	0.042	0.042
Ce*	0.184	0.184	0.184	0.323	0.323	0.014	0.054	0.054	D.L.	D.L.	D.L.
Hf	0.271	D.L.	D.L.	D.L.	0.178	0.162	0.216 (0.082)	D.L.	0.114	0.057	0.140 (0.051)
Ta	1.01 (0.06)	0.99	0.91 (0.01)	0.89	1.57 (0.01)	1.06	0.35 (0.02)	D.L.	D.L.	0.33 (0.10)	0.30 (0.20)

Table 4. (Continued)

	88-48C	88-45D	88-45E	88-74C	88-74D	88-74E	88-85C	88-85D	88-58A	88-58B	88-58C
(wt.%)											
SiO_2	46.56 (0.45)	47.02 (0.46)	47.02 (0.46)	46.73 (0.10)	46.73 (0.10)	46.73 (0.10)	47.04 (0.58)	47.04 (0.58)	47.30 (0.48)	47.30 (0.48)	47.30 (0.48)
TiO_2	0.38 (0.01)	0.78 (0.03)	0.78 (0.03)	0.75 (0.04)	0.75 (0.04)	0.75 (0.04)	0.92 (0.06)	0.92 (0.06)	0.91 (0.09)	0.91 (0.09)	0.91 (0.09)
Al_2O_3	34.68 (0.08)	34.84 (0.21)	34.84 (0.21)	33.57 (0.37)	33.57 (0.37)	33.57 (0.37)	33.87 (0.53)	33.87 (0.53)	33.06 (0.36)	33.06 (0.36)	33.06 (0.36)
$FeO^{\#}$	1.56 (0.02)	1.24 (0.27)	1.24 (0.27)	2.53 (0.05)	2.53 (0.05)	2.53 (0.05)	1.27 (0.13)	1.27 (0.13)	1.63 (0.31)	1.63 (0.31)	1.63 (0.31)
MgO	1.16 (0.01)	1.13 (0.03)	1.13 (0.03)	1.06 (0.15)	1.06 (0.15)	1.06 (0.15)	1.25 (0.08)	1.25 (0.08)	1.42 (0.19)	1.42 (0.19)	1.42 (0.19)
Na_2O	1.21 (0.07)	1.38 (0.04)	1.38 (0.04)	1.18 (0.42)	1.18 (0.42)	1.18 (0.42)	1.21 (0.21)	1.21 (0.21)	0.70 (0.11)	0.70 (0.11)	0.70 (0.11)
K_2O	9.89 (0.04)	8.94 (0.16)	8.94 (0.16)	8.69 (0.76)	8.69 (0.76)	8.69 (0.76)	9.26 (0.17)	9.26 (0.17)	10.46 (0.09)	10.46 (0.09)	10.46 (0.09)
F	D.L.	0.102 (0.013)	0.102 (0.013)	0.070	0.070	0.070	0.134 (0.012)	0.134 (0.012)	0.150 (0.029)	0.150 (0.029)	0.150 (0.029)
Cl	0.006 (0.008)	D.L.	D.L.	0.010	0.010	0.010	0.010	0.010	D.L.	D.L.	D.L.
Total	95.44	95.38	95.38	94.56	94.56	94.56	94.90	94.90	95.58	95.58	95.58
(ppm)											
Li		79	78 (2)	36 (7)	46 (6)	46	89 (10)	74 (14)	37	43 (5)	
Ca	D.L.	344	374	295 (5)	437 (72)	357	565 (164)	513 (56)	339 (101)	465 (4)	
Sc	15.7 (6.9)	D.L.	14.4 (6.0)	15.4 (3.3)	25.1	17.1	8.2	7.2 (0.3)	10.3 (1.2)	17.0 (1.5)	D.L.
V	252 (41)	280	294 (22)	220 (32)	274 (29)	229	312 (22)	252 (13)	156 (2)	177 (41)	11.6
Cr	353	160	128	95 (7)	D.L.	110	188 (3)	160 (44)	83 (15)	D.L.	124
Mn	2.1	D.L.	1.3 (0.1)	12.3 (5.2)	10.5 (1.8)	9.7	3.4 (0.5)	2.6 (0.2)	3.6 (0.0)	4.8 (1.2)	134
Co	2.89	0.84	1.06 (0.24)	5.19 (0.65)	4.72 (0.72)	4.22	1.94 (0.54)	1.94 (0.49)	3.22 (0.03)	2.99 (0.15)	5.8
Ni		1.96	2.13	8.84 (1.06)	10.09 (0.53)	9.80	2.57 (0.46)	2.05 (0.20)	7.38 (0.61)	8.39 (0.66)	2.29
Cu		2.77	2.77	0.99 (0.11)	1.40 (0.08)	0.79	1.35 (0.34)	1.36 (0.04)	1.31 (0.74)	1.10	7.17
Zn*	6	20	20	12	12	12	24	24	27	27	27
Rb		280	312	197 (18)	210 (4)	215	322	376 (23)	251 (8)	275 (20)	
Sr	D.L.	237	289 (13)	69 (11)	81 (17)	67	303 (32)	311 (8)	143 (4)	252 (9)	120
*Y**	D.L.	0.07	0.07	0.08	0.08	0.08	0.14	0.14	0.03	0.03	0.03
*Zr**	0.25	1.15	1.15	0.85	0.85	0.85	1.14	1.14	2.06	2.06	2.06
Nb	18.8 (3.6)	2.0	1.9 (0.3)	12.8 (3.0)	15.1 (2.5)	15.0	4.0 (0.6)	4.0 (0.1)	18.6 (4.9)	23.7 (0.8)	D.L.
Cs		2.46	3.64	0.89 (0.10)	0.80 (0.21)	0.92	3.33	4.93 (0.33)	6.89 (0.73)	4.79 (0.51)	
Ba	832 (139)	1966 (253)	1828	900 (53)	1155 (194)	1050 (76)	2331 (287)	2131 (124)	598 (10)	784 (58)	618
*La**	0.014	0.010	0.010	0.004	0.004	0.004	0.033	0.033	0.007	0.007	0.007
*Ce**	0.038	0.080	0.080	0.005	0.005	0.005	0.021	0.021			
Hf	0.077 (0.001)	0.075 (0.007)	D.L.	0.134 (0.011)	0.120 (0.024)	0.136	0.180 (0.030)	0.182 (0.028)	0.116 (0.029)	0.192 (0.028)	D.L.
Ta	0.34 (0.07)	0.09 (0.04)	0.03	0.35 (0.08)	0.43 (0.09)	0.46 (0.14)	0.14 (0.05)	0.12 (0.04)	1.39	1.32 (0.08)	D.L.

Notes: # Total Fe as FeO. * For these elements the lowest value within a sample is reported because of fractionation during laser ablation (Zn) and contamination from micro-inclusions (Y, Zr and REE). D.L. and blank represent data below detection limits and elements not determined, respectively. Italicized elements are present in concentrations lower than 3 times detection limits in most analyses. Values in parentheses are standard deviations at 1σ level.

Table 5. Stoichiometries of biotite.

	87-81F	87-81I	87-81K	87-83C	87-83D	87-86F	88-32A	88-32B	87-279D	87-279F	87-279G	88-48C	88-45D	88-45E	88-74C	88-74D	88-74E	88-85C	88-85D	88-58A	88-58B	88-58C
Tetrahedral sites																						
Si	5.584	5.583	5.584	5.523	5.523	5.591	5.492	5.492	5.543	5.544	5.544	5.506	5.578	5.579	5.478	5.479	5.479	5.488	5.488	5.451	5.451	5.452
^{IV}Al	2.416	2.417	2.416	2.477	2.477	2.409	2.508	2.508	2.457	2.456	2.456	2.494	2.422	2.421	2.522	2.521	2.521	2.512	2.512	2.549	2.549	2.548
Octahedral sites																						
Ti	0.177	0.177	0.177	0.177	0.177	0.183	0.177	0.177	0.185	0.185	0.185	0.133	0.188	0.188	0.236	0.236	0.236	0.188	0.188	0.240	0.240	0.240
^{VI}Al	0.676	0.675	0.676	0.635	0.633	0.731	0.660	0.660	0.645	0.647	0.647	0.782	0.830	0.830	0.673	0.673	0.674	0.761	0.760	0.631	0.632	0.634
Fe[#]	2.519	2.519	2.520	2.445	2.445	2.415	2.801	2.802	2.237	2.237	2.237	1.775	2.019	2.020	2.134	2.134	2.134	2.012	2.012	2.615	2.615	2.616
Mg	2.272	2.272	2.272	2.355	2.355	2.405	2.044	2.045	2.502	2.503	2.502	3.015	2.659	2.659	2.605	2.605	2.605	2.733	2.733	2.131	2.131	2.132
Mn	2.6E-02	2.2E-02	1.6E-02	1.6E-02	1.6E-02	1.6E-02	8.8E-03	9.0E-03	2.2E-02	1.7E-02	1.6E-02	5.1E-04	5.5E-04	6.3E-04	3.7E-03	3.8E-03	3.5E-03	6.7E-03	7.0E-03	2.6E-03	2.6E-03	2.7E-03
Li	2.6E-03	2.6E-03	3.3E-03	3.3E-03	2.4E-03	4.2E-03	2.2E-03	2.2E-03	3.0E-03	3.0E-03	3.1E-03	2.6E-03	7.5E-03	7.3E-03	4.8E-03	5.4E-03	5.0E-03	8.3E-03	7.5E-03	4.5E-03	4.7E-03	4.7E-03
Sc	3.8E-04	3.2E-04	2.6E-04	2.4E-04	2.6E-04	3.5E-04	2.4E-04	2.6E-04	2.9E-04	4.1E-04	4.5E-04	2.2E-04	1.1E-04	1.2E-04	2.9E-04	2.8E-04	2.5E-04	9.4E-05	1.0E-04	2.6E-04	2.5E-04	2.4E-04
V	3.5E-03	3.8E-03	2.6E-03	2.5E-03	2.5E-03	2.6E-03	3.3E-03	3.5E-03	1.2E-02	1.2E-02	1.2E-02	2.6E-03	3.8E-03	4.0E-03	4.4E-03	4.3E-03	4.6E-03	4.5E-03	4.5E-03	2.3E-03	2.0E-03	1.8E-03
Cr	3.1E-03	3.5E-03	3.2E-03	1.6E-03	1.7E-03	1.9E-03	1.6E-03	1.5E-03	3.4E-03	3.0E-03	3.2E-03	D.L.	6.5E-03	5.8E-03	5.8E-03	5.7E-03	5.1E-03	5.9E-03	6.3E-03	3.0E-03	3.3E-03	3.0E-03
Co	7.8E-04	7.0E-04	6.3E-04	7.3E-04	7.5E-04	7.6E-04	6.1E-04	6.2E-04	3.0E-04	2.6E-04	3.3E-04	7.5E-04	3.9E-04	3.9E-04	1.7E-03	1.7E-03	1.6E-03	4.7E-04	5.3E-04	8.0E-04	6.6E-04	5.9E-04
Ni	1.4E-03	1.4E-03	1.4E-03	2.5E-03	2.3E-03	1.7E-03	1.0E-03	1.1E-03	6.1E-04	7.4E-04	9.7E-04	1.5E-04	9.4E-04	8.9E-04	4.3E-03	3.9E-03	4.2E-03	7.0E-04	7.0E-04	1.7E-03	1.6E-03	1.6E-03
Cu	1.2E-02	8.6E-05	8.3E-05	8.3E-05	9.4E-05	D.L.	6.5E-05	D.L.	D.L.	8.0E-05	7.8E-05	5.0E-05	9.9E-05	9.9E-05	1.0E-04	8.3E-05	9.2E-05	1.0E-04	9.3E-05	8.2E-05	7.1E-05	7.5E-05
Zn	2.5E-03	2.5E-03	2.5E-03	4.5E-03	4.5E-03	4.0E-03	1.1E-03	1.1E-03	2.9E-03	2.9E-03	2.9E-03	1.0E-03	7.7E-03	7.7E-03	3.5E-03	3.5E-03	3.5E-03	5.5E-03	5.5E-03	6.5E-03	6.5E-03	6.5E-03
Y	1.7E-06	1.5E-06	1.7E-06	2.6E-06	2.6E-06	2.8E-06	1.5E-06	1.5E-06	1.6E-06	1.6E-06	1.6E-06	D.L.	7.8E-07	7.8E-07	D.L.	D.L.	D.L.	6.8E-07	6.8E-07	3.9E-07	3.9E-07	3.9E-07
Zr	9.8E-07	9.8E-07	9.8E-07	D.L.	D.L.	D.L.	8.1E-07	8.1E-07	9.6E-07	9.6E-07	9.6E-07	1.2E-06	1.4E-06	1.4E-06	1.1E-06	1.1E-06	1.1E-06	1.3E-06	1.3E-06	1.5E-06	1.5E-06	1.5E-06
Nb	4.7E-04	5.5E-04	3.8E-04	3.8E-04	5.8E-04	4.5E-04	3.9E-04	3.4E-04	3.4E-04	3.3E-04	3.4E-04	2.1E-04	8.7E-06	7.7E-06	1.8E-04	1.8E-04	1.7E-04	1.1E-05	1.3E-05	2.3E-04	2.5E-04	1.5E-06
Hf	5.8E-07			D.L.		3.4E-07	3.2E-07			2.7E-07		8.1E-08	2.4E-07	1.2E-07	5.6E-08	5.0E-08	9.0E-08	3.8E-07	3.8E-07	D.L.	D.L.	D.L.
Ta	1.9E-05	2.0E-05	1.5E-05	1.5E-05	2.0E-05	1.5E-05	4.8E-06	D.L.	1.2E-05	7.3E-06	5.4E-06	4.2E-06	2.4E-07	1.5E-07	5.2E-06	5.0E-06	5.1E-06	3.8E-07	3.8E-07	1.2E-05	1.5E-05	D.L.
X_{Mg}	0.474	0.474	0.474	0.491	0.491	0.499	0.422	0.422	0.528	0.528	0.528	0.629	0.568	0.568	0.550	0.550	0.550	0.576	0.576	0.449	0.449	0.449
Total	5.683	5.682	5.682	5.643	5.641	5.766	5.701	5.700	5.614	5.612	5.611	5.711	5.723	5.724	5.677	5.677	5.677	5.720	5.720	5.640	5.640	5.638
Al^{TOT}	3.092	3.092	3.092	3.111	3.111	3.140	3.168	3.168	3.102	3.103	3.103	3.276	3.252	3.252	3.195	3.195	3.195	3.272	3.272	3.181	3.181	3.181
Interlayer sites																						
Ca	D.L.	7.4E-03	9.6E-03	D.L.	6.3E-03	7.4E-03	5.6E-03	D.L.	D.L.	6.2E-03	D.L.	D.L.	6.5E-03	6.7E-03	5.2E-03	4.9E-03	5.7E-03	5.2E-03	5.4E-03	6.6E-03	4.7E-03	D.L.
Na	D.L.	D.L.	D.L.	0.100	0.100	D.L.	D.L.	D.L.	D.L.	D.L.	D.L.	0.135	0.118	0.118	0.154	0.154	0.154	0.118	0.118	0.115	0.115	0.115
K	1.787	1.787	1.787	1.831	1.831	1.846	1.803	1.803	1.891	1.892	1.892	1.756	1.458	1.458	1.752	1.752	1.752	1.592	1.592	1.860	1.860	1.861
Rb	D.L.	2.9E-03	D.L.	D.L.	3.5E-03	2.6E-03	2.6E-03	D.L.	D.L.	2.0E-03	2.6E-03	D.L.	4.1E-03	4.3E-03	3.3E-03	2.9E-03	3.0E-03	4.1E-03	3.8E-03	2.8E-03	2.4E-03	D.L.
Sr	2.0E-05	2.2E-05	1.8E-05	1.3E-05	1.3E-05	1.3E-05	2.7E-05	D.L.	2.1E-05	1.5E-05	2.0E-05	2.0E-05	2.4E-05	1.9E-05	2.0E-05	2.6E-05	1.8E-05	4.7E-05	5.5E-05	5.0E-05	5.5E-05	3.9E-05
Cs	D.L.	1.6E-04	1.7E-04	2.6E-04	2.6E-04	1.6E-04	8.1E-05	8.1E-05	D.L.	1.4E-04	1.4E-04	D.L.	3.0E-04	3.3E-04	8.2E-05	6.9E-05	7.0E-05	2.6E-04	3.1E-04	2.2E-04	2.1E-04	D.L.
Ba	8.0E-03	8.6E-03	8.6E-03	6.9E-03	7.9E-03	5.8E-03	6.7E-03	8.5E-03	7.1E-03	6.0E-03	7.4E-03	2.7E-03	5.2E-03	4.4E-03	3.8E-03	4.0E-03	4.0E-03	7.1E-03	7.8E-03	2.6E-03	2.6E-03	2.4E-03
La	1.5E-06	1.5E-06	1.5E-06	2.5E-06	2.5E-06	D.L.	6.7E-07	6.7E-07	3.6E-06	3.6E-06	3.6E-06	3.8E-06	7.7E-07	7.2E-07	8.9E-08	8.9E-08	8.9E-08	4.9E-07	4.9E-07	9.9E-07	9.9E-07	9.9E-07
Ce	4.1E-06	4.1E-06	2.4E-06	2.4E-06	2.4E-06	D.L.	1.2E-06	1.2E-06	6.3E-06	6.3E-06	6.3E-06	6.1E-06	2.2E-06	2.2E-06	1.4E-07	1.4E-07	1.4E-07	1.1E-06	1.1E-06	1.2E-06	1.2E-06	1.2E-06
X_{Na}				0.052	0.052							0.071	0.075	0.075	0.081	0.081	0.081	0.069	0.069	0.058	0.058	0.058
Total	1.795	1.806	1.808	1.938	1.949	1.862	1.817	1.811	1.898	1.906	1.902	1.893	1.592	1.592	1.919	1.918	1.919	1.726	1.727	1.987	1.985	1.978

Notes: Stoichiometries are based upon 22 O and site occupancies are assigned on the basis of ionic radius arguments. [#] Total Fe as FeO. $X_{Mg} = Mg/(Mg + Fe^{TOT})$; $X_{Na} = Na/(Na + K)$.
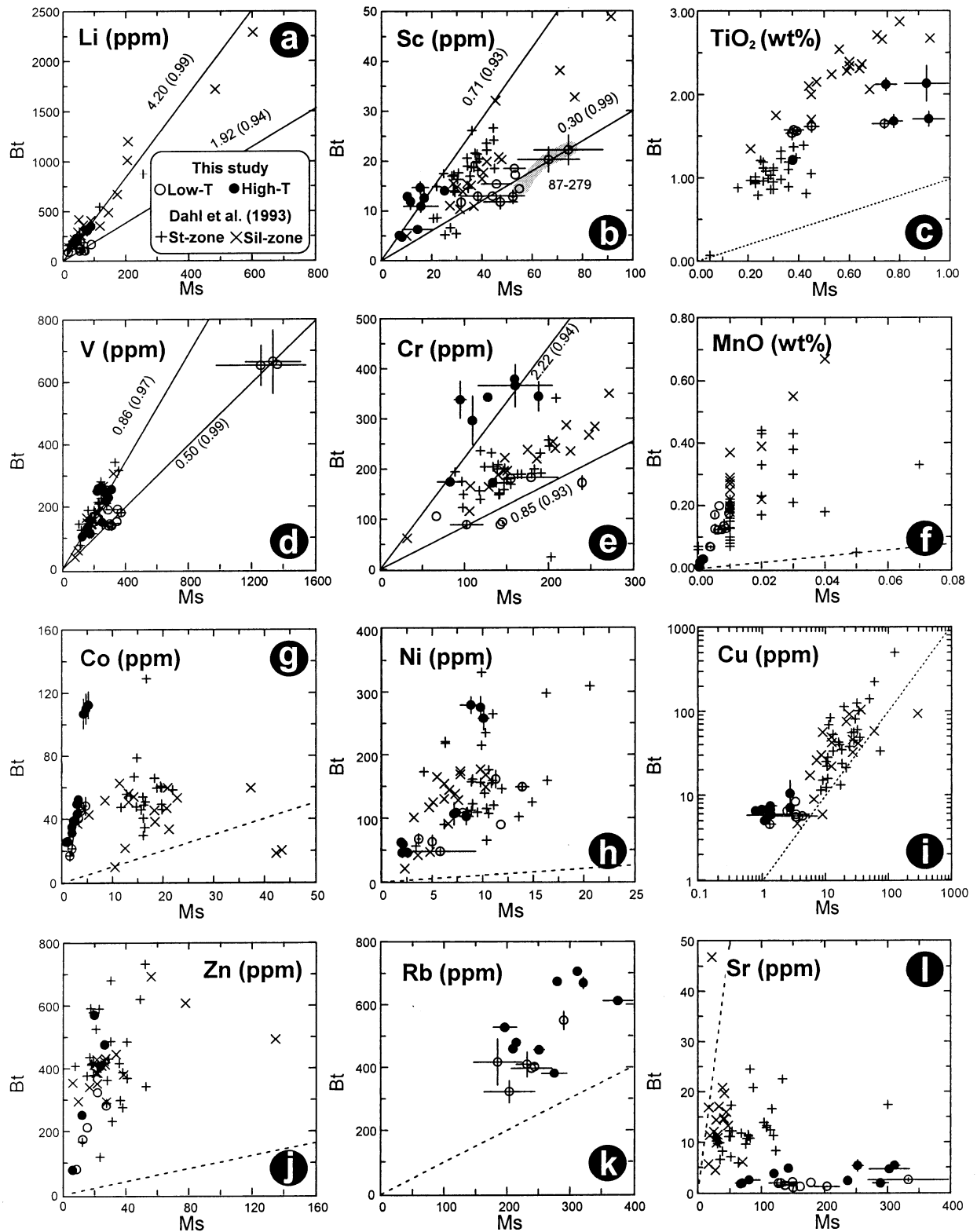
Table 6. Stoichiometries of muscovite.

	87-81F	87-81I	87-81K	87-83C	87-83D	87-86F	88-32A	88-32B	87-279D	87-279F	87-279G	88-48C	88-45D	88-45E	88-74C	88-74D	88-74E	88-85C	88-85D	88-58A	88-58B	88-58C
Tetrahedral sites																						
Si	6.218	6.215	6.217	6.202	6.198	6.268	6.222	6.223	6.237	6.236	6.237	6.183	6.197	6.197	6.248	6.247	6.247	6.241	6.242	6.284	6.283	6.284
^{iv}Al	1.782	1.785	1.783	1.798	1.802	1.732	1.778	1.777	1.763	1.764	1.763	1.817	1.803	1.803	1.752	1.753	1.753	1.759	1.758	1.716	1.717	1.716
Octahedral sites																						
Ti	0.039	0.039	0.039	0.038	0.038	0.045	0.037	0.037	0.074	0.074	0.074	0.038	0.077	0.077	0.075	0.075	0.075	0.091	0.091	0.091	0.091	0.091
^{vi}Al	3.586	3.580	3.584	3.574	3.565	3.569	3.527	3.529	3.491	3.488	3.490	3.611	3.610	3.610	3.538	3.537	3.537	3.539	3.541	3.461	3.461	3.462
$Fe^{\#}$	0.194	0.194	0.194	0.187	0.187	0.199	0.234	0.234	0.177	0.177	0.177	0.174	0.136	0.136	0.283	0.283	0.283	0.141	0.141	0.182	0.182	0.182
Mg	0.215	0.215	0.215	0.227	0.226	0.249	0.230	0.230	0.256	0.256	0.256	0.229	0.221	0.221	0.210	0.210	0.210	0.248	0.248	0.282	0.282	0.282
Mn	7.5E-04	1.1E-03	6.0E-04	6.0E-04	8.5E-04	7.1E-04	4.4E-04	4.1E-04	1.1E-03	8.9E-04	9.6E-04	3.0E-05	D.L.	1.8E-05	1.8E-04	1.5E-04	1.4E-04	4.8E-05	3.7E-05	5.1E-05	6.8E-05	8.3E-05
Li	1.4E-03	1.4E-03	1.5E-03	1.2E-03	1.2E-03	2.0E-03	3.7E-04		1.1E-03	1.1E-03	1.2E-03	2.8E-04	1.7E-03	1.6E-03	7.6E-04	9.7E-04	9.7E-04	1.8E-03	1.5E-03	7.7E-04	8.9E-04	
Sc	9.4E-04	8.1E-04	6.8E-04	5.6E-04	9.3E-04	9.5E-04	7.8E-04		9.5E-04	1.2E-03	1.3E-03	2.8E-04	D.L.	2.5E-04	2.7E-04	4.4E-04	3.0E-04	1.4E-04	1.2E-04	1.8E-04	2.9E-04	2.0E-04
V	4.5E-03	5.4E-03	4.7E-03	4.9E-03	4.6E-03	4.8E-03	5.8E-03	5.4E-03	2.1E-02	2.0E-02	1.9E-02	3.9E-03	4.3E-03	4.5E-03	3.4E-03	4.2E-03	3.5E-03	4.7E-03	3.8E-03	2.4E-03	2.7E-03	1.9E-03
Cr	D.L.	D.L.	D.L.	2.2E-03	2.4E-03	1.6E-03	1.6E-03	D.L.	D.L.	3.6E-03	2.7e-03	5.4E-03	2.4E-03	2.4E-03	1.9E-03	D.L.	1.7E-03	2.8E-03	2.4E-03	1.2E-03	1.2E-03	2.0E-03
Co	4.2E-05	5.0E-05	4.5E-05		6.3E-05	4.8E-05	3.0E-05		D.L.	2.0E-05	2.5E-05	3.9E-05	1.1E-05	1.4E-05	6.9E-05	6.3E-05	5.6E-05	2.5E-05	2.5E-05	4.3E-05	3.9E-05	3.0E-05
Ni	D.L.	1.6E-04		1.5E-04	1.9E-04	1.1E-04	4.9E-05		D.L.	7.7E-05	6.7E-05	D.L.	2.6E-05	2.8E-05	1.2E-04	1.4E-05	1.3E-04	3.4E-05	2.7E-05	9.8E-05	1.1E-04	9.5E-05
Cu	4.3E-05	4.4E-05	D.L.	D.L.	3.1E-05	1.5E-05	1.7E-05	D.L.	D.L.	5.3E-05	4.2E-05	D.L.	3.4E-05	3.4E-05	1.2E-05	1.7E-05	9.7E-06	1.6E-05	1.7E-05	1.6E-05	1.3E-05	D.L.
Zn	1.5E-04	1.5E-04	1.5E-04	2.7E-04	2.7E-04	3.4E-04	1.0E-04	1.0E-04	1.9E-04	1.9E-04	1.9E-04	7.3E-05	2.4E-04	2.4E-04	1.5E-04	1.5E-04	1.5E-04	2.8E-04	2.8E-04	3.2E-04	3.2E-04	3.2E-04
Y	3.0E-06	3.0E-06	3.0E-06	2.5E-06	2.5E-06	1.5E-06	2.4E-06	2.4E-06	7.6E-07	7.6E-07	7.6E-07	D.L.	5.9E-07	5.9E-07	7.2E-07	7.2E-07	7.2E-07	1.2E-06	1.2E-06	2.4E-07	2.4E-07	2.4E-07
Zr	1.0E-06	1.0E-06	3.0E-06	4.6E-06	4.6E-06	1.6E-06	1.4E-06	1.4E-06	2.0E-06	2.0E-06	2.0E-06	2.1E-06	9.8E-06	9.8E-06	7.4E-06	7.4E-06	7.4E-06	9.6E-06	3.3E-05	1.8E-05	1.8E-05	1.8E-05
Nb	2.2E-04	D.L.	2.3E-04	2.3E-04	3.5E-04	2.4E-04	2.2E-04	D.L.	D.L.	1.93E-04	1.6E-04	1.6E-04	1.7E-05	1.6E-05	1.1E-04	1.3E-04	1.3E-04	3.3E-05	3.3E-05	1.6E-04	1.6E-04	2.0E-04
Hf	1.2E-06	D.L.	D.L.	D.L.	8.0E-07	7.3E-07	9.5E-07	D.L.	5.0E-07	2.5E-07	6.1E-07	3.4E-07	3.3E-07	D.L.	5.9E-07	5.3E-07	6.0E-07	7.8E-07	7.9E-07	5.0E-07	8.4E-07	D.L.
Ta	4.5E-06	4.4E-06	4.0E-06	3.9E-06	6.9E-06	4.7E-06	1.5E-06	D.L.	D.L.	1.4E-06	1.3E-06	1.5E-06	3.7E-07	1.5E-07	1.5E-06	1.9E-06	2.0E-06	5.8E-07	5.0E-07	6.0E-06	5.7E-06	D.L.
X_{Mg}	0.526	0.526	0.526	0.548	0.548	0.556	0.496	0.496	0.591	0.591	0.591	0.569	0.619	0.619	0.426	0.426	0.426	0.637	0.637	0.609	0.609	0.609
Total	4.042	4.038	4.043	4.035	4.027	4.072	4.038	4.038	4.021	4.023	4.023	4.061	4.053	4.054	4.113	4.112	4.113	4.030	4.030	4.021	4.020	4.021
Al^{TOT}	5.368	5.365	5.367	5.371	5.368	5.301	5.305	5.306	5.254	5.252	5.253	5.428	5.413	5.413	5.290	5.290	5.290	5.298	5.298	5.178	5.177	5.178
Interlayer sites																						
Ca	D.L.	1.4E-02	D.L.	D.L.	D.L.	1.5E-02	1.4E-02	D.L.	D.L.	2.0E-02	1.1E-02	D.L.	6.7E-03	7.2E-03	5.8E-03	8.6E-03	7.0E-03	1.1E-02	9.9E-03	6.6E-03	9.0E-03	D.L.
Na	0.225	0.224	0.224	0.249	0.249	0.230	0.171	0.171	0.231	0.231	0.231	0.311	0.352	0.352	0.306	0.306	0.306	0.311	0.311	0.181	0.181	0.181
K	1.699	1.698	1.698	1.712	1.710	1.719	1.816	1.817	1.728	1.727	1.727	1.676	1.503	1.503	1.482	1.482	1.482	1.567	1.567	1.773	1.773	1.773
Rb	D.L.	1.3E-03	D.L.	1.6E-03	D.L.	1.4E-03	D.L.	D.L.	D.L.	1.1E-03	1.0E-03	D.L.	1.5E-03	1.7E-03	1.1E-03	1.1E-03	1.2E-03	1.7E-03	2.0E-03	1.4E-03	1.5E-03	D.L.
Sr	1.2E-03	1.4E-03	1.4E-03	1.9E-03	D.L.	1.5E-03	3.0E-03	D.L.	1.6E-03	2.6E-03	1.2E-03	D.L.	2.1E-03	2.6E-03	6.2E-04	7.2E-04	6.0E-04	2.7E-03	2.7E-03	1.4E-03	1.3E-03	1.1E-03
Cs	D.L.	8.7E-06	5.4E-06	1.6E-05	1.0E-05	6.0E-06		D.L.	D.L.	1.1E-05	1.2E-05	D.L.	1.8E-05	2.6E-05	5.8E-06	5.8E-06	6.7E-06	2.4E-05	3.5E-05	5.0E-05	3.4E-05	D.L.
Ba	3.3E-02	4.2E-02	3.4E-02	2.3E-02	3.6E-02	2.9E-02	2.5E-02		2.4E-02	2.3E-02	2.2E-02	4.8E-03	1.1E-02	1.0E-02	5.2E-03	6.6E-03	6.0E-03	1.3E-02	1.2E-02	3.4E-03	4.4E-03	3.5E-03
La	D.L.	D.L.	D.L.	D.L.	D.L.	1.6E-07	3.3E-07	3.3E-07	2.4E-07	2.4E-07	2.4E-07	7.8E-08	5.6E-08	5.6E-08	2.4E-08	2.4E-08	2.4E-08	1.8E-07	1.8E-07	4.1E-08	4.1E-08	D.L.
Ce	1.0E-06	1.0E-06	1.0E-06	1.8E-06	1.8E-06	8.1E-08	3.0E-07	3.0E-07	D.L.	D.L.	D.L.	2.2E-07	4.4E-07	4.4E-07	2.6E-08	2.6E-08	2.6E-08	1.2E-07	1.2E-07	D.L.	D.L.	D.L.
X_{Na}	0.117	0.117	0.117	0.127	0.127	0.118	0.086	0.086	0.118	0.118	0.118	0.157	0.190	0.190	0.171	0.171	0.171	0.166	0.166	0.093	0.093	0.093
Total	1.958	1.981	1.957	1.985	1.999	1.996	2.030	2.015	1.984	2.004	1.994	1.992	1.876	1.877	1.801	1.805	1.803	1.906	1.905	1.967	1.971	1.959

Notes: Stoichiometries are based upon 22 O and site occupancies are assigned on the basis of ionic radius arguments. #Total Fe as FeO. $X_{Mg} = Mg/(Mg + Fe^{TOT})$; $X_{Na} = Na/(Na + K)$.

Fig. 2. Distribution diagrams showing the partitioning of elements between coexisting biotite (Bt) and muscovite (Ms). Open and closed circles represent low and high-T biotite-muscovite pairs, respectively. + and × represent mica pairs from St and Sil-zone, reported by Dahl et al. (1993). Error bars represent the standard deviation at 1σ. Data are regressed where they show systematic differences between low and high-T. The numbers are slopes of regression lines, with values in parentheses representing r^2. Dashed lines represent equal partitioning. Labeled data points are discussed in the text.
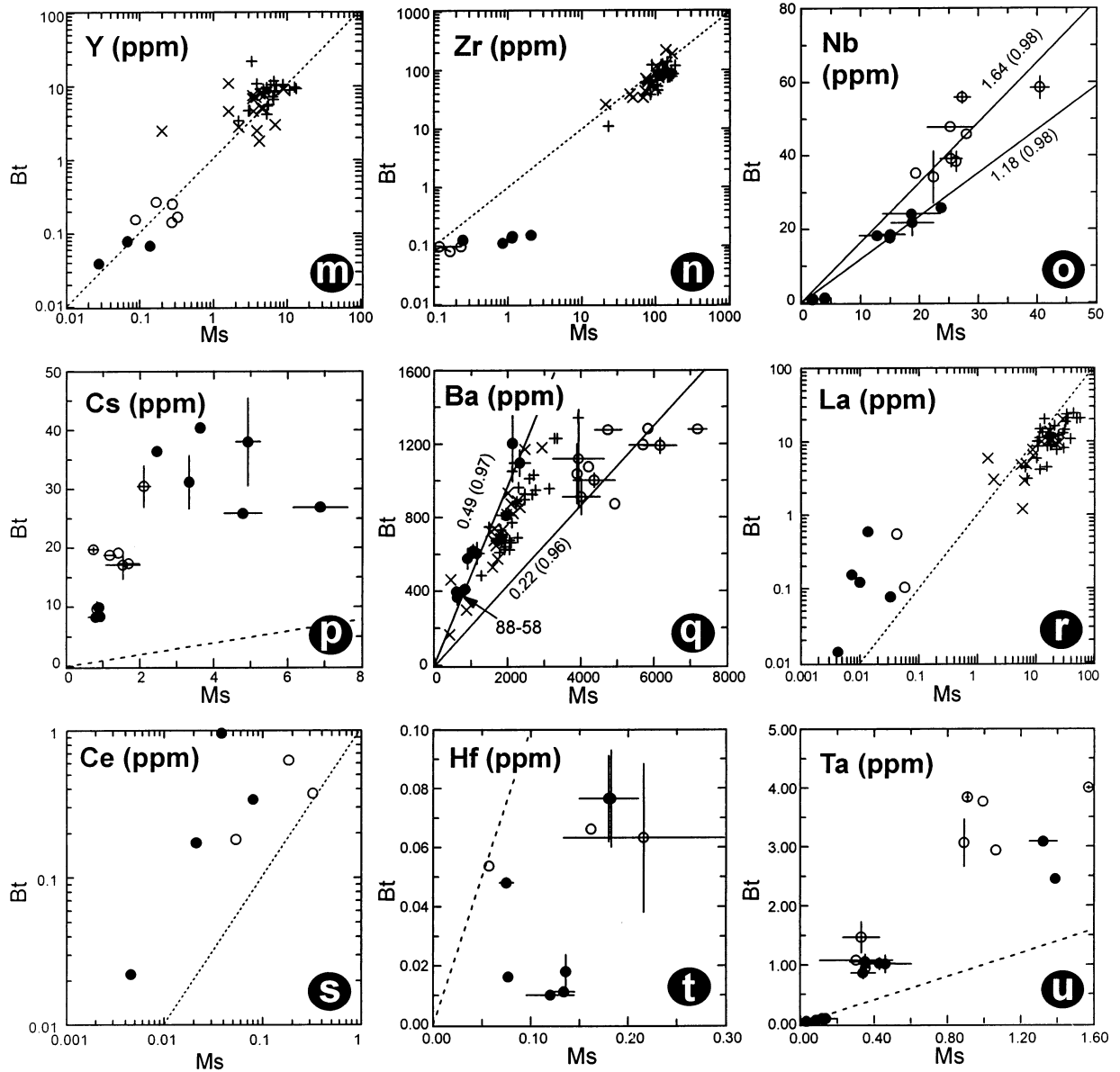
Fig. 2. (Continued)

and muscovite are presented in Tables 3–4 as averages and standard deviations (1σ) of 2–3 analyses performed for each mineral from two to three domains in a thin-section, except for sample 87–86, in which all analyses come from a single domain. Most analyses of Ca, Y, Zr, La, Ce and Hf in biotite and Ca, Ni, Cu, Y, Zr, La, Ce and Hf in muscovite are close to their respective lower limits of detection (<3 times detection limit) and these elements are italicized in the Tables 3–4. Mica stoichiometries are given in Tables 5–6. Cation site-occupancies were assigned on the basis of ionic radii (Shannon, 1976).

Establishing the presence or absence of zoning is important for an evaluation of chemical equilibrium. Each mineral, therefore, was analyzed close to its rim and at the core for representative samples. The analyzed micas are virtually unzoned both in major and trace element concentrations. Care was taken to avoid obvious cleavages during laser ablation, but cleavage does not appear to affect analytical results.

4. MAJOR ELEMENT COMPOSITIONS

Structural formulae for both biotite and muscovite are based on 22 oxygen atoms (Tables 5–6). Both biotite and muscovite show no significant variation in Si and thus Al^{IV} content, which is defined as the difference between 8.0 and the number of Si atoms. All of our micas are saturated with respect to Ti because of their coexistence with either ilmenite or rutile. In the case of Al, micas from high-T samples, except for sample 88–58, are saturated in Al because of the presence of kyanite in the matrix (Tables 5–6). However, there are no Al-saturating phases in the low-T samples. Fe^{3+}/Fe^{2+} ratios in biotite and muscovite were

Table 7. Molar partition coefficients (D_i^*) of coexisting biotite-muscovite pairs from metapelites, western Labrador.

Elements	87-81F	87-81I	87-81K	87-83C	87-83D	87-86F	88-32A	88-32B	87-279D	87-279F	87-279G
Octahedral sites											
Li		1.18	1.09	1.80	1.37 (0.23)	1.40	4.01 (0.28)			1.77 (0.51)	1.69
Sc	0.27	0.25	0.26 (0.02)	0.27	0.18 (0.02)	0.25	0.19 (0.03)	0.22	0.20	0.23 (0.05)	0.22 (0.05)
V	0.50	0.33	0.37 (0.08)	0.33	0.35 (0.01)	0.35	0.37 (0.04)	0.42	0.36	0.37 (0.07)	0.39 (0.09)
Cr			0.88	0.46	0.48	1.21	0.66 (0.14)			0.53	0.76
Co	12.26	9.25	9.26		7.67 (1.01)	10.43	13.22 (0.95)			8.41 (4.12)	8.29 (3.98)
Ni		5.77		10.59	7.95 (0.48)	10.24	13.97 (1.82)			6.12 (3.73)	9.31
Cu	1.87	1.30			1.94		2.59 (0.64)			0.96 (0.68)	1.19
Zn	10.46	10.46	10.46	10.89	10.89	7.73	7.02	7.01	10.18	10.12	10.12
Y	0.39	0.39	0.39	0.67	0.67	1.21	0.40	0.40	1.32	1.31	1.31
Zr	0.62	0.62	0.62				0.37	0.37	0.31	0.31	0.31
Nb	1.44		1.56 (0.09)	1.09	1.07 (0.07)	1.25	1.18 (0.11)			1.14	1.35
Hf						0.31	0.22 (0.12)			0.70	
Ta		2.88	3.21 (0.08)	2.56	1.89 (0.01)	2.10	2.04 (0.14)			3.31 (1.15)	2.65
Interlayer sites											
Rb		1.89			2.11 (0.11)	1.88	2.02 (0.25)			1.76 (0.40)	2.51 (0.68)
Sr	0.02	0.02		0.01	0.01 (0.001)	0.01	0.01 (0.002)		0.01	0.01 (0.002)	0.02 (0.004)
Cs		18.12	30.50 (5.93)		16.14 (2.31)	15.46	13.27 (1.84)			12.43 (4.18)	11.44
Ba	0.24	0.20	0.25	0.30	0.21 (0.02)	0.20	0.26 (0.04)	0.31	0.29	0.25 (0.04)	0.32 (0.09)
La							2.04	2.04	14.55	14.46	14.45
Ce	3.90	3.90	3.90	1.29	1.29		3.86	3.86			
T (°C)	507	507	507	492	492	503	503	503	530	530	530
P (kbar)	7.6	7.6	7.6	7.7	7.7	7.4	8.8	8.8	8.8	8.8	8.8

Italicized elements are present in concentrations below or close to 3 times detection limits in either biotite or muscovite. Metamorphic temperatures and pressures were estimated using the garnet-biotite geothermometer of Holdaway et al. (1997), and Grt-Pl-Bt-Ms and Grt-Ky-Qtz-Pl geobarometers of Hodges and Crowley (1985).

not determined, precluding full evaluation of the variation of trace element distributions involving iron.

4.1. Biotite

The majority of the VI-fold sites are filled by Mg (2.04–3.01 atoms per formula unit, p.f.u.) and Fe^{TOT} (1.77–2.80 atoms p.f.u.) (Table 5). X_{Mg} of biotite, ranging from 0.42 to 0.64, reflects variation both in the bulk composition and T. Octahedral Al in biotite, defined as the difference between Al^{TOT} and ^{IV}Al, is between 0.63 and 0.83 atoms p.f.u. Most of the Al^{IV} is balanced by Al^{VI}, suggesting operation of the Al-Tschermaks substitution, $(Fe, Mg)SiAl_{-1}^{VI}Al_{-1}^{IV}$. Biotite coexisting with kyanite is relatively enriched in Al^{TOT} (3.18–3.28) compared to low-T biotite (3.09–3.17), presumably due to Al saturation in the former samples (Table 5). Ti contents in biotite range from 0.13 to 0.24 atoms p.f.u. with no clear correlation with the contents of Fe and Mg and metamorphic grade (Table 5). Concentrations of Mn are typically low, but vary widely (31–1,541 ppm). In all of the biotites studied, the sum of the octahedral cations is below the theoretical value of six atoms p.f.u., but is always above 5.61, implying no significant amount of Fe^{3+} in the biotites.

Theoretically, two atoms p.f.u. are allocated to the XII-interlayer site in biotite. The XII- site in the analyzed biotites is dominated by K (1.46–1.89 atoms p.f.u.) with small amounts of Na (0.10–0.15 atoms p.f.u.) and Ca (<0.01 atoms p.f.u.) (Table 5). The amount of interlayer site vacancy, ranging from 0.02 to 0.41 atoms p.f.u., is surprising given the almost complete analyses. Concentrations of F in biotite range between 0.10 and 0.28 atoms p.f.u. Cl contents are uniformly low (<0.04 atoms p.f.u.).

4.2. Muscovite

Al^{VI} of muscovite varies from 3.46 to 3.61 atoms p.f.u. with the lowest value from the high grade sample 88-58. Al comprises 88% of the ions on average in the octahedral sites, the remainder being mostly Mg (0.21–0.28 atoms p.f.u.) and Fe^{TOT} (0.14–0.28 atoms p.f.u.). The muscovite compositions deviate slightly from the ideal Al-Tschermak substitution when defined in terms of Si and Al^{TOT}. However, the linear distribution of analyses parallel to the Al-Tschermak substitution (not shown) indicates no significant variations in Fe^{3+} contents among the analyzed muscovites. With the exception of sample 88–58 (which does not contain kyanite), the content of Al^{TOT} of muscovite from high-T samples is similar to that of low-T samples, indicating quasi-saturation of Al in low-T samples. The Ti contents of muscovite range from 0.04 to 0.09 cations p.f.u., and correlate positively with the Mg content. The Mn content of all muscovites studied is extremely low (1.3–76.7 ppm) and appears to decrease with metamorphic grade. The total octahedral occupancy of analyzed muscovites (ideally 4.00 atoms p.f.u.) varies from 4.02 to 4.11 atoms p.f.u., indicating slight deviation from dioctahedral micas in all analyses.

The XII interlayer site in white mica is filled predominantly by K (1.48–1.82 atoms p.f.u.) and by lesser amounts of Na (0.17–0.35 atoms p.f.u.). The Ca content determined by LAM-ICP-MS is negligible (mostly below detection limits, occasion-

Table 7. (Continued)

Elements	88-48C	88-45D	88-45E	88-74C	88-74D	88-74E	88-85C	88-85D	88-58A	88-58B	88-58C
Octahedral sites											
Li		2.98	2.93 (0.22)	4.04 (1.64)	3.58 (0.49)	3.32	2.86 (0.34)	3.09	3.78	3.40	
Sc	0.51 (0.23)		0.32 (0.14)	0.70 (0.16)	0.41	0.54	0.43	0.52 (0.04)	0.93	0.55 (0.09)	0.77
V	0.44 (0.09)	0.59	0.59 (0.06)	0.84 (0.13)	0.66 (0.08)	0.83	0.60 (0.04)	0.76).07)	0.63	0.48 (0.11)	0.63
Cr		1.78	2.01	2.62 (0.34)		1.99	1.34 (0.12)	1.68 (0.50)	1.57		0.96
Co	12.47	22.89	18.53 (4.36)	15.93 (2.35)	17.14 (3.03)	18.63	11.91 (3.46)	13.26 (3.67)	12.16	10.85 (1.14)	12.68
Ni		23.73	20.73	23.23 (2.99)	18.81 (1.65)	20.69	13.15 (3.16)	16.51 (3.16)	11.02	9.17 (1.38)	11.16
Cu		1.92	2.82	4.98 (0.58)	3.08 (0.18)	6.07	4.05 (1.15)	3.58	3.29	3.40	
Zn	9.37	21.31	21.31	15.31	15.31	15.31	12.53	12.52	13.43	13.43	13.44
Y		0.86	0.86				0.36	0.36	1.05	1.05	1.05
Zr	0.37	0.09	0.09	0.09	0.09	0.09	0.09	0.09	0.05	0.05	0.05
Nb	0.84 (0.21)	0.34	0.33 (0.06)	1.04 (0.25)	0.90 (0.15)	0.87	0.21 (0.07)	0.25 (0.07)	0.97	0.82	
Hf	0.15	0.48		0.06 (0.01)	0.06	0.10	0.31 (0.08)	0.31 (0.08)			
Ta	1.83 (0.41)	0.42 (0.21)	0.65	2.20 (0.58)	1.75 (0.39)	1.610.55	0.41 (0.16)	0.48 (0.18)	1.32	1.75	
Interlayer sites											
Rb		2.70	2.54	2.95 (0.28)	2.41 (0.07)	2.46	2.29	1.79	2.04	1.55	
Sr		0.01	0.01 (.001)	0.03 (.007)	0.03 (.008)	0.03	0.02 (.002)	0.02 (.002)	0.04	0.02 (.005)	0.04
Cs		16.60	12.47	12.35 (1.42)	11.41 (3.07)	10.05	10.31	8.50 (1.76)	4.39	6.06	
Ba	0.54 (0.10)	0.46 (0.06)	0.42	0.71 (0.08)	0.58 (0.11)	0.650.06	0.52 (0.07)	0.62 (0.11)	0.74	0.58 (0.05)	0.67
La	47.24	13.48	13.48	3.60	3.60	3.60	2.56	2.56	23.47	23.48	23.48
Ce	27.34	4.77	4.77	5.34	5.34	5.34	8.95	8.95			
T (°C)	622	643	643	658	658	658	656	656	680	680	680
P (kbar)	9.4	9.4	9.4	8.0	8.0	8.0	8.0	8.0	12.5	12.5	12.5

Italicized elements are present in concentrations below or close to 3 times detection limits in either biotite or muscovite. Metamorphic temperatures and pressures were estimated using the garnet-biotite geothermometer of Holdaway et al. (1997), and Grt-Pl-Bt-Ms and Grt-Ky-Qtz-Pl geobarometers of Hodges and Crowley (1985).

ally up to 0.02 atoms p.f.u.). The total occupancy of the interlayer site ranges from 1.80 to 2.02 and is not related to metamorphic grade. Deficiencies in the XII-sites in muscovite, even when trace elements are included in the analyses, may be partially explained by the H_3OK_{-1} and NH_4K_{-1} substitutions and by vacancies in XII-sites due to charge balance constraints caused by other substitutions in IV, VI and XII-sites (Guidotti and Sassi, 1998a; Guidotti and Sassi, 1998b). The analyzed muscovites have less than 0.06 atoms of F p.f.u. with a strong positive dependence on Mg content. Most Cl concentrations are below detection limits.

5. THERMODYNAMICS OF TRACE ELEMENT DISTRIBUTION

The partitioning behaviour of trace elements can be considered in terms of exchange reactions involving major element cations for which the thermodynamic basis is well established (e.g., Kretz, 1961). For example, partitioning of the trace element Cs and the major element K between coexisting biotite and muscovite may be expressed by the exchange reaction:

$$Cs_2^{XII}Mg_6^{VI}Al_2^{IV}Si_6^{IV}O_{20}(OH)_4 + K_2^{XII}Al_4^{VI}Al_2^{IV}Si_6^{IV}O_{20}(OH)_4 =$$
Cs-Bt   K-Ms
$$K_2^{XII}Mg_6^{VI}Al_2^{IV}Si_6^{IV}O_{20}(OH)_4 + Cs_2^{XII}Al_4^{VI}Al_2^{IV}Si_6^{IV}O_{20}(OH)_4$$
K–Bt   Cs–Ms

$$(1)$$
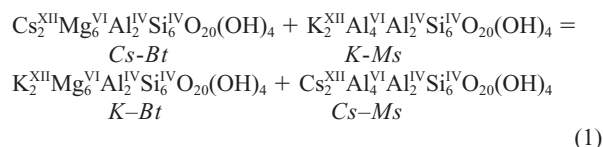
At equilibrium,

$$\mu_{Cs-Bt} + \mu_{K-Ms} = \mu_{K-Bt} + \mu_{Cs-Ms} \qquad (2)$$

where μ_{Cs-Bt} is the chemical potential of endmember Cs-Bt, which is related to the concentration by

$$\mu_{Cs-Bt} = G_{Cs-Bt} + RTlnX_{Cs-Bt}\gamma_{Cs-Bt} \qquad (3)$$

Here G_{Cs-Ba} is the molar Gibbs energy of pure endmember Cs-Bt, R is the gas constant, γ_{Cs-Bt} is an activity coefficient, and X_{Cs-Bt} is the mole fraction, Cs/(Cs+K) in biotite. By introducing three additional equations analogous to Eqn. (3) and substituting them into Eqn. (2), we obtain

$$K_D^{Cs-K} = \left[\frac{X_{Cs}}{X_K}\right]^{Bt} \Big/ \left[\frac{X_{Cs}}{X_K}\right]^{Ms} = \left[\frac{\gamma_K}{\gamma_{Cs}}\right]^{Bt}\left[\frac{\gamma_{Cs}}{\gamma_K}\right]^{Ms}\left\{\exp\left(\frac{-\Delta G°}{RT}\right)\right\}$$
$$(4)$$

where K_D^{Cs-K} is the distribution coefficient for Cs in K-biotite/K-muscovite, and $\Delta G°$ is the Gibbs energy difference in reaction (1) with all components pure. In dilute solutions, the activity coefficients are expected to remain constant following Henry's Law. Therefore, the concentration ratio will also remain constant by the Gibbs-Duhem equation. $\Delta G°$ is thus mainly dependent on variations in T. The effects of P are predicted to be small owing to very small changes in the volume of reaction as a result of the exchange reactions. Because X_{K-Bt} and X_{K-Ms} are very nearly 1.0, the distribution coefficient on the left may be written X_{Cs-Bt}/X_{Cs-Ms}. Hence, for a very low concentration of Cs, we would expect a linear relation between X_{Cs-Bt} and X_{Cs-Ms} at constant temperature.

6. THE DISTRIBUTION OF TRACE ELEMENTS

The abundance ranges and partitioning behaviour of the trace elements among the 22 biotite-muscovite pairs are presented in

Table 8. Comparison of the Nernst distribution coefficients (D_i) between biotite and muscovite with those of previous studies.

Facies	This study		Dahl et al. (1993)	Domanik et al. (1993)	Dutrow et al. (1986)	Butler (1967)	Moorbath et al. (1968)
	U. Greenschist	Amphibolite	Amphibolite	Ep. Blueschist	Amphibolite	U. Greenschist	Amphibolite
Methods	LAM-ICP-MS		Solution ICP-MS	SIMS	AA	Spectrography	Isotope Dilution
Octahedral sites							
Mn	20.62 (5.73)	24.18 (9.64)	16.96 (7.22)				
Li	2.38 (1.22)	4.49 (0.56)	5.31 (1.47)		4.57 (0.68)		
Sc	0.31 (0.04)	0.77 (0.24)	0.49 (0.12)				
V	0.50 (0.06)	0.86 (0.18)	0.88 (0.15)				
Cr	0.95 (0.34)	2.35 (0.67)	1.30 (0.32)				
Co	13.04 (2.51)	20.41 (5.05)	3.45 (2.15)				
Ni	12.15 (3.71)	22.68 (7.30)	18.03 (7.93)				
Cu	2.18 (0.79)	4.98 (1.68)	2.52 (1.53)				
Zn	12.73 (2.11)	20.00 (4.76)	17.77 (10.43)				
Y	1.02 (0.57)	1.07 (0.41)	1.94 (2.15)				
Zr	0.58 (0.19)	0.15 (0.12)	0.74 (0.25)				
Nb	1.67 (0.22)	0.89 (0.45)					
Hf	0.55 (0.34)	0.28 (0.21)					
Ta	3.43 (0.72)	1.68 (0.93)					
Interlayer sites							
Na	0.47 (0.11)	0.28 (0.03)	0.21 (0.11)				
Rb	1.80 (0.25)	2.07 (0.40)		2.08		1.85 (0.78)	1.52
Sr	0.01 (0.00)	0.02 (0.01)	0.32 (0.33)	0.03			0.40
Cs	14.81 (5.64)	9.21 (3.26)					
Ba	0.23 (0.04)	0.53 (0.09)	0.44 (0.34)	0.57		0.42 (0.05)	
La	8.48 (6.12)	13.11 (12.70)	0.72 (0.55)				
Ce	2.76 (1.10)	8.03 (7.04)					
Ca	0.37 (0.09)	0.65 (0.19)	2.07 (1.09)			0.48 (0.08)	

The data of Dahl et al. (1993) represent an average of the St- and Sil-zones. Values in parentheses represent standard deviations at 1σ level. Abbreviations: SIMS; secondary ion mass spectrometry, AA: atomic absorption spectrophotometry.

Figure 2 (a–u). Also included for comparison in these plots are data from Dahl et al. (1993) who reported ICP solution analyses of separates from 49 coexisting biotite-muscovite pairs from the staurolite and sillimanite zones in the Black Hills of South Dakota. The partition coefficients are presented here both as ppm concentration ratios

$$D_i = \frac{ppm\ Bt}{ppm\ Ms} \quad (5)$$

equivalent to Nernst distribution coefficients, and as atomic or molar partition coefficients

$$D_i^* = \frac{X_i^{Bt}}{X_i^{Ms}} \quad (6)$$

following the terminology of Beattie et al. (1993). In these relationships, i refers to a specific element and X_i is the mole fraction of component i in biotite or muscovite on a specific site, calculated on the basis of two interlayer sites, eight tetrahedral sites, and either six or four octahedral sites for biotite and muscovite, respectively. D_i^* values between coexisting biotite and muscovite determined in this study are listed in Table 7, with their corresponding standard deviations (1σ). Metamorphic P-T were estimated using garnet-plagioclase-biotite-muscovite and garnet-kyanite-quartz-plagioclase geobarometers of Hodges and Crowley (1985) and garnet-biotite geothermometry of Holdaway et al. (1997) (Table 7). Garnet-biotite geo-

thermometers incorporating significant corrections for calcium in garnet, such as those of Hoinkes (1986), Williams and Grambling (1990) and the TWQ program, version 2.02 (Berman, 1991) invariably yield unreasonably high temperatures for low-T samples which contain garnet enriched in calcium (~0.2 mole fraction) compared to high-T garnets (<0.1 mole fraction). There is a temperature gap between low- and high-T samples, which may correspond to the missing staurolite-biotite zone noted above. As discussed above, distribution coefficients of Ni, Cu, Y, Zr, La, Ce and Hf involve relatively high analytical errors because of their concentrations in either biotite or muscovite or both approach detection limits. The distribution coefficients for these elements, therefore, should be considered as only rough estimates.

6.1. Trace Element Distribution

For the trace elements, it is evident from Figure 2 that:

1. Li, Mn, Co, Ni, Cu, Zn, Rb, Nb, Cs, La, Ce and Ta prefer biotite over muscovite regardless of metamorphic grade;
2. At low-T, Cr and Y partition coefficients are nearly equal between the micas; and
3. Sc, V, Cr (high-T), Sr, Zr, Ba and Hf favour muscovite.

The distributions of Li, Sc, V, Cr, Nb and Ba show systematic differences between low- and high-T micas (Figs. 2a,b,d,e,o,q). The factors governing these differences are discussed in a later
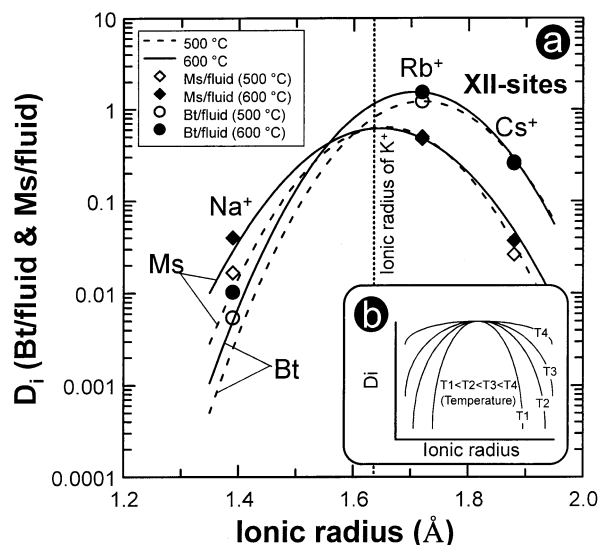
Fig. 3. (a) Crystal-fluid partition coefficient vs. ionic radius for interlayer cations in phlogopite and muscovite. Data are from Volfinger (1976). Curves are calculated from Eqn. (5). Dotted line indicates ionic radius of K^+. (b) Schematic diagram showing the predicted decrease of slopes with increasing temperature.

section. The decreasing concentrations of Sc, Mn and Y in micas with metamorphic grade (Figs. 2b,f,m) indicate that the matrix is progressively depleted in these elements, probably because of the increasing modal abundance of garnet, which is known to strongly sequester them. The distribution of Ti between biotite and muscovite is strongly controlled by X_{Mg} of muscovite (not shown).

As indicated by the thermodynamic considerations above, the systematic linear distributions of most trace elements at similar metamorphic grade, together with the measured distributions intersecting at the origin (Fig. 2), suggest a close approach to chemical equilibrium between coexisting biotite and muscovite across the range of bulk-rock composition and metamorphic grade. In addition, there is no evidence that any of the trace elements departs from Henry's Law behaviour.

However, it is noteworthy that biotite and muscovite from sample 87-279 show variations in Sc ranging from 14 to 22 and from 55 to 74 ppm, respectively, but with similar distribution coefficients (Fig. 2b). Analytical errors can be ruled out, because they are especially low for Sc due to its abundance well above the detection limits in both biotite and muscovite, and the absence of spectral interferences. The variability in Sc concentrations at the thin-section scale may be attributed to mosaic equilibrium (initially defined by Zen, 1963), which is caused by limited diffusion ranges of the element under the metamorphic conditions. Kretz et al. (1999) also reported evidence for different domains of equilibrium for specific trace elements, which they attributed to variations in the magnitudes of deformation and recrystallization, together with different diffusion rates.

6.2. Contamination

Most trace elements in the micas show similar abundance ranges when compared to the data of Dahl et al. (1993), but Zr,
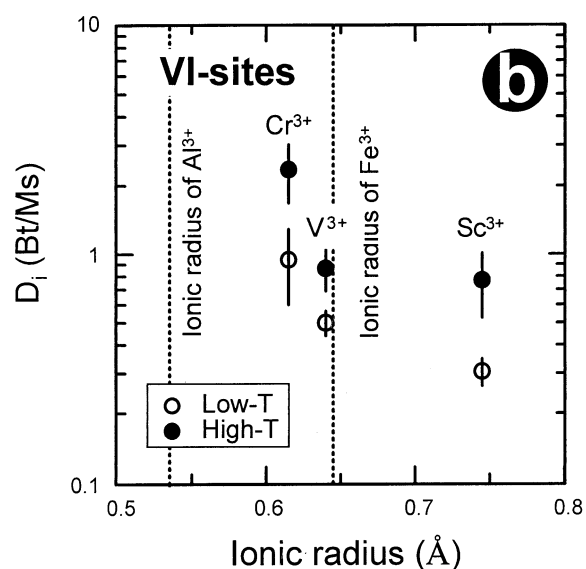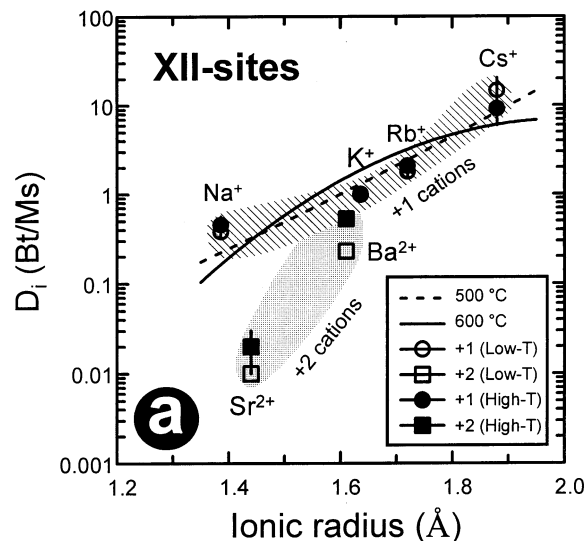
Fig. 4. Relationship between distribution coefficient and ionic radius. (a) D_i values for low and high-T micas plotted against ionic radius for monovalent and divalent cations in XII-interlayer sites (shaded areas), along with distribution lines for 500 and 600°C (solid and dashed lines) calculated from the data of Volfinger (1976). (b) D_i values of 3+ cations in VI-sites plotted against corresponding ionic radius. For reference, ionic radii of Al^{3+} and Fe^{3+} ions are shown.

La and Ce are much lower in our analyses (Fig. 2n,r,s). This result is clearly due to contamination from zircons and monazite in their samples, which are difficult to remove from mineral separates. Moreover, consistently lower contents of Mn and Co in muscovite and higher Ca and Sr contents in biotite from our data (Figs. 2f,g,l; Table 3) indicate that there may have been other important sources of contamination in Dahl et al.'s data. High Mn and Co in muscovite analyses of Dahl et al. (1993) may be attributed to contamination by ilmenite, despite their efforts to remove it using a high strength magnetic field. They reported that Sr data of their muscovite were contaminated by oligoclase and applied corrections using Sr contents in oligo-
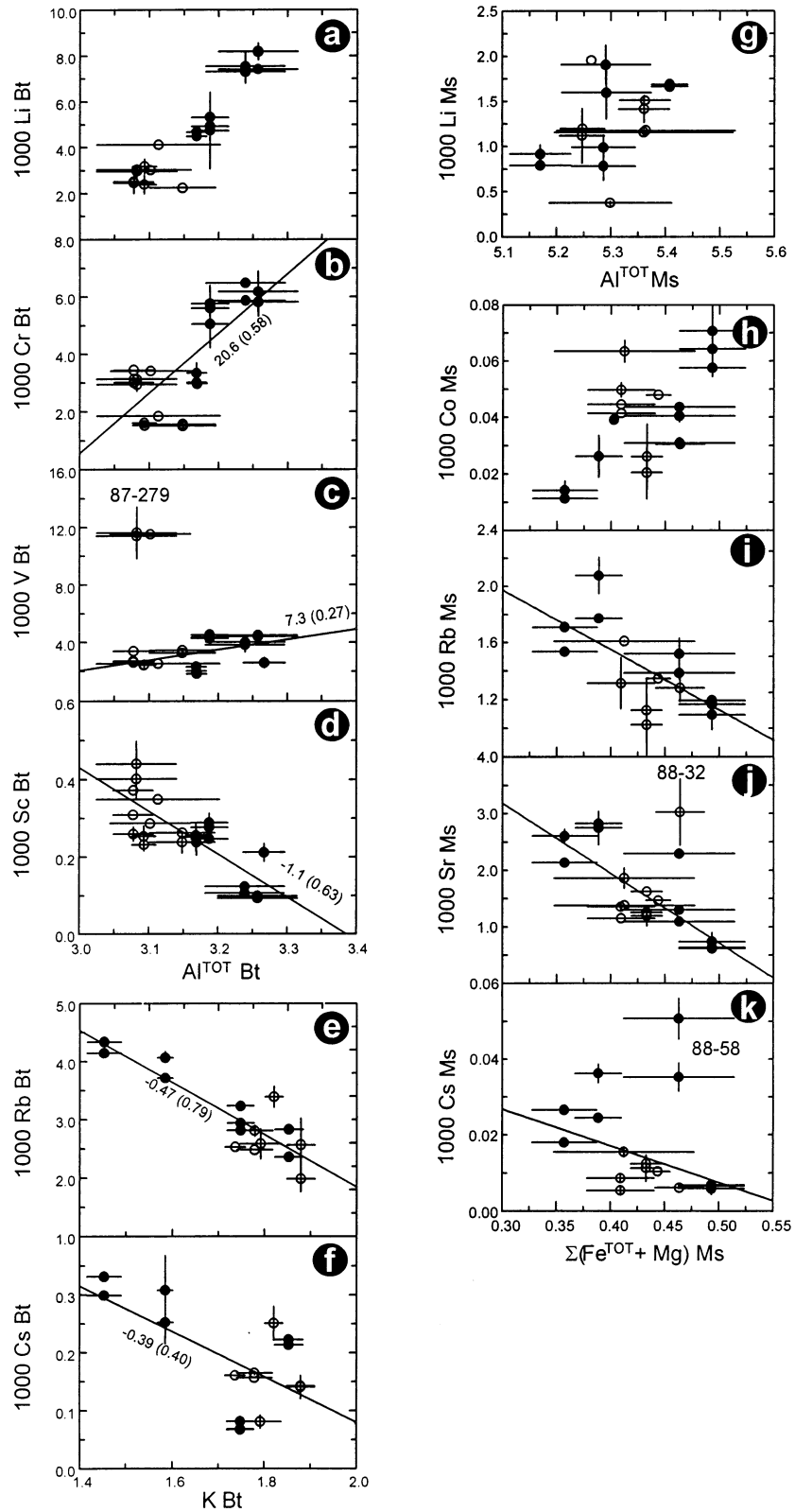
Fig. 5. (a–d) The concentrations of Li, Cr, V and Sc versus Al^{TOT} in biotite. Note that the effects of Al^{TOT} on the contents of Cr, V and Sc are different. (e–f) The concentrations of Rb and Cs in biotite versus K contents. (g) Li in muscovite versus Al^{TOT}. (h–k) Co, Rb, Sr and Cs versus $\Sigma(Fe^{TOT}+Mg)$ of muscovite. Open and closed circles represent low and high-T samples, respectively. Regression lines are shown, and the numbers represents slope of regression lines, with r^2 in parentheses, where these are significant.

clase. However, significantly higher Sr contents in biotite, together with high Ca contents in the biotites of Dahl et al. (1993), indicate that their biotite analyses were also probably contaminated by oligoclase (Fig. 2l). Bea et al. (1993) reported a similar difference between LAM-ICP-MS and mineral separate analyses for biotite. Their solution ICP-MS analyses for REE, Th, U, Y, Sr, Zr, Cu and Zn were consistently higher, by almost two orders of magnitude, than results from analyzing the same crystals in thin section with a LAM-ICP-MS.

6.3. Comparison

The measured distribution coefficients from this study are compared with other data from pelitic rocks, most of which represent amphibolite facies conditions, except for those of Butler (1967) which are for greenschist facies conditions (Table 8). In Table 8, the data of Dahl et al. (1993) and Butler (1967) are averages of their staurolite and sillimanite-zones samples, and samples with no epidote, respectively. Overall, the trace element distributions and relative enrichment patterns are consistent with published analyses of coexisting biotite and muscovite (e.g., Butler, 1967; Moorbath et al., 1968; Dutrow et al., 1986; Hervig and Peacock, 1989; Dahl et al., 1993; Domanik et al., 1993). However, there are important differences between this and previous studies.

The average D_{Li}, D_V and D_{Ba} values of high-T samples show good agreement with those of Dahl et al. (1993) (Table 8). The average D_{Li} value of high-T samples also shows excellent agreement with that of Dutrow et al. (1986). The measured D_{Ba} value from high-T samples is similar to values reported for epidote-bearing blueschists from the Franciscan Complex by Domanik et al. (1993) within permitted errors, implying no significant pressure or bulk composition dependence on Ba distribution (Table 8). However, the D_{Ba} value of Butler (1967), which was obtained from an upper greenschist facies pelite, is higher than that of our low-T samples (Table 8). Distribution coefficients of Li, V and Ba between biotite and muscovite increase with metamorphic grade (Table 8).

For Sc and Cr, the distribution coefficients of Dahl et al. (1993), which are from a metamorphic grade equivalent to our high-T samples, are close to our low-T samples (Table 8). A close examination of the plots for Sc and Cr from Dahl et al. (1993) reveals that their staurolite-zone data are close to our high-T data, but their sillimanite zone data overlap with the low-T data from this study (Fig. 2b, e). In addition, on the basis of the observed trend for V partitioning between biotite and muscovite in this study, the partitioning of Sc and Cr are expected to increase with T. However, the opposite trends in the data of Dahl et al. (1993) may indicate that their Sc and Cr compositions from the sillimanite-zone micas were re-equilibrated at lower temperatures, or that their data were influenced by an increasing amount of secondary (retrograde) micas in the sillimanite-zone.

Our distribution coefficients for Ca, Co and Sr differ significantly from those Dahl et al. (1993), probably because of contamination in either biotite or muscovite in their analyses as mentioned above. In support of this assertion, D_{Sr} of Domanik et al. (1993), which was determined by the SIMS technique, shows a good agreement with our high-T results (Table 8). On the other hand, D_{Sr} values determined by a bulk mineral anal-

ysis method such as employed by Dahl et al. (1993) and Moorbath et al. (1968) are 10 times higher.

Partitioning of Rb between biotite and muscovite is within the range of values reported in the literature and shows little variation through the entire range of bulk composition and metamorphic grade. Mn, Ni, Cu and Zn data from Dahl et al. (1993) plot on or very close to our trends (Fig. 2). For the distribution of Nb, Hf, Ta and Cs between coexisting micas, no published data from pelitic micas are available for comparison.

The comparison of data given above enables us to conclude that our partition coefficients are more reliable than the results from several previous studies which were obtained by means of bulk analysis of mineral separates. Assuming an equilibrium distribution of trace elements, as is suggested by our data, we now discuss the distribution behaviour of trace elements in terms of various structural, compositional or thermal controls on element partitioning.

7. FACTORS INFLUENCING THE DISTRIBUTION COEFFICIENTS

7.1. Crystal Structural Effects

Crystal-melt partitioning behaviour of trace elements for various minerals has been modeled in terms of the lattice strain associated with placing a cation on a particular crystallographic site when the radius of the cation differs from the optimal radius for that site (e.g., Onuma et al. 1968; Möller 1988; Blundy and Wood, 1991, 1994; Beattie, 1994; Brenan et al., 1995). Trace element partitioning in mica-melt and mica-fluid systems also shows that the incorporation of a trace element into the crystal lattice is controlled by the size mismatch between the trace and host cations in the mica structures (Jensen, 1973; Matsui et al., 1977; Iiyama, 1979; Volfinger and Robert, 1980; LaTourrette et al., 1995). Using the phlogopite-fluid and muscovite-fluid partition coefficients experimentally measured by Volfinger (1976) at 500 and 600°C at a constant pressure of 1 kbar, we test the model in order to develop analogous relations that describe biotite/muscovite partition coefficients in terms of the ionic radius of the substituting trace elements.

We assume, for example for reaction (1), that $\Delta G_{exchange}$ can be approximated by the energy required to remove a Cs^+ ion from the biotite and insert it into the crystal lattice of muscovite while simultaneously transferring a K^+ ion from muscovite to biotite. The structural work required to incorporate a Cs^+ into the muscovite is the sum of ΔG_{strain}, the lattice strain due to size mismatch between the radius of Cs^+ and the optimum radius (r_o) of the XII-site in muscovite, and $\Delta_{relaxation}$, the energy liberated when a Cs^+ ion is removed from the lattice site in biotite, assuming major element substitution contributes a negligible amount of ΔG_{strain} and $\Delta G_{relaxation}$ because of its similarity in ionic radius to the optimum size of the crystallographic site.

Following the method of Blundy and Wood (1994), we have fitted the partitioning data of Volfinger (1976) by non-linear least-squares regression to the relation:

$$D(P,T,X) = D_o(P,T,X)$$
$$\cdot \exp\left[\frac{-4\pi E N_A}{RT}\left\{\frac{r_o}{2}(r_i - r_o)^2 + \frac{1}{3}(r_i - r_o)^3\right\}\right] \quad (7)$$
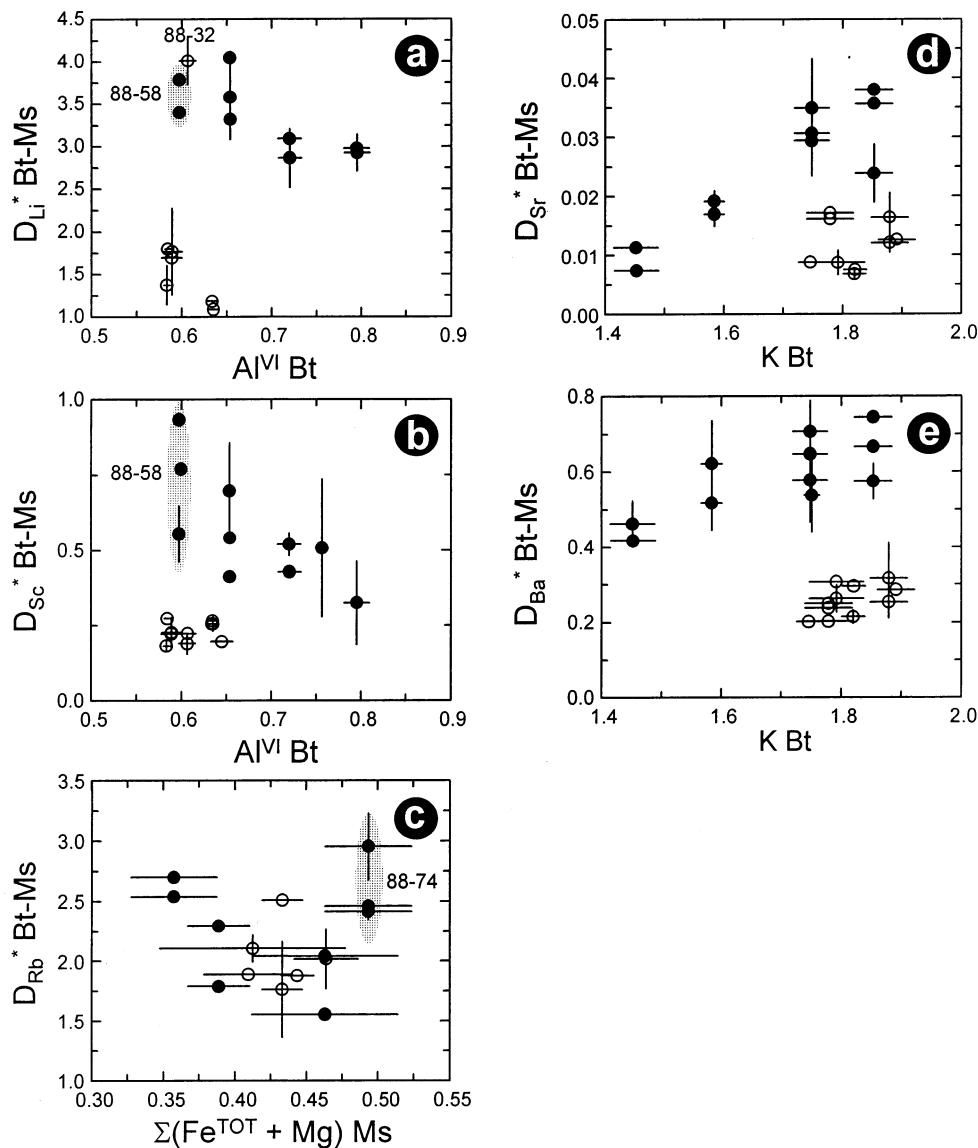
Fig. 6. (a–e) Major element compositional effects of Al^{VI}, $\Sigma(Fe^{TOT}+Mg)$ and K of either biotite or muscovite on the distribution of Li, Sc, Rb, Sr and Ba between biotite and muscovite. All of the trace elements except for Rb show two different trends with metamorphic grade. Open and closed circles represent low and high-T, respectively.

which relates the partition coefficient, $D(P,T,X)$, for a given cation of ionic radius r_i, at a particular condition of P, T and bulk composition, to the partition coefficient, $D_o(P,T,X)$, for a cation whose radius equals the optimal site radius, r_o. In this relation, E is the value of Young's modulus for the site, N_A is Avogadro's number, R is the gas constant and T is in Kelvins. The data and associated fits using Eqn. (7) are shown in Figure 3 in which the slope of the parabola is a function of E. Partition coefficients for elements substituting into XII-sites in biotite and muscovite decrease as the cation size misfit increases, consistent with incorporation of the trace element becoming less favourable with increasing lattice strain. Variations in $D_i^{Ms-fluid}$ with T are greater for Na and Cs than for Rb (Fig. 3a), consistent with the ionic radius of Rb being close to the ideal radius for the site (Fig. 3b). For $D_i^{Bt-fluid}$, in contrast, the

pattern is different, with Cs partitioning showing the least effect of T. This is not in accord with expectations, since the ionic radius of Rb is close to the ideal radius for the site, suggesting that it should show the least variation with T. Although we are unable to unambiguously explain this result, we suspect that it may be due to poor quality analytical data for Cs for the biotite experiments.

It is noteworthy that the derived peak value for r_o for 1+ cations in biotite is slightly larger than that for muscovite. In biotite, the peak r_o coincides with the radius of Rb^+ ion. In contrast, in muscovite the peak closely corresponds to the radius of the K^+ ion. This difference in optimum ionic radius of XII-sites between biotite and muscovite is compatible with the fact that ideal trioctahedral biotite has a completely filled octahedral sheet (filled by the relatively large Fe^{2+} and Mg^{2+}
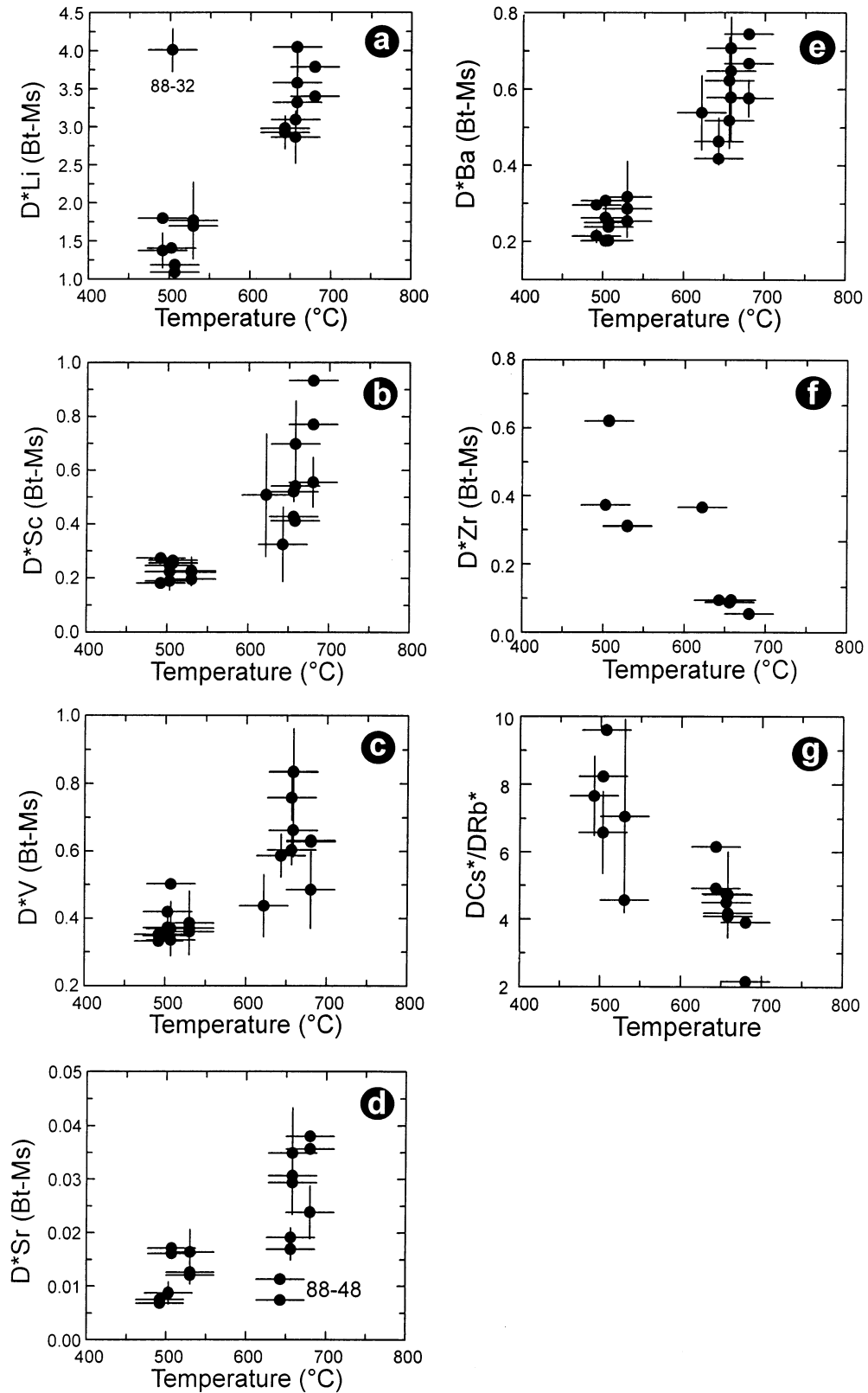
Fig. 7. (a–g) Plots of D^*_{Li}, D^*_{Sc}, D^*_{V}, D^*_{Sr}, D^*_{Cs}, D^*_{Ba}, D^*_{Zr} and D^*_{Cs}/D^*_{Rb} against metamorphic temperatures estimated using the garnet-biotite geothermometer.

cations), whereas ideal muscovite has smaller and fewer octa-hedral sites as a result of the tetrahedral rotation necessary to accommodate the size mismatch between the IV and VI-sheets (Guidotti and Sassi, 1998b). The decreasing slopes of the curve for +1 cations in XII-sites of muscovite, as the temperature increases from 500 to 600°C, may indicate variations in ther-mal expansivity with T (Fig. 3). If this is true, we would expect more significant thermal effects for elements away from the optimum ionic radius. The slopes of parabolas for XII-sites in biotite do not appear to change with T.

On the basis of biotite-fluid and muscovite-fluid partitioning, the distributions of trace elements between coexisting biotite and muscovite would be expected to vary systematically with ionic radius, if lattice strain were a major controlling factor. Fig. 4a shows the curve for D_i^{Bt-ms}, derived by dividing the values for $D_i^{Bt-fluid}$ by those for $D_i^{ms-fluid}$ in Fig. 3, together with our data. Overall, our partitioning data for Na, K, Rb and Cs fit the modeled biotite-muscovite partitioning curves very well, demonstrating controls of ionic radius on solid-solid partitioning. It is evident from Fig. 4a that cations Ba^{2+} (1.61 Å), Sr^{2+} (1.44 Å) and Na^+ (1.39 Å) favour muscovite with its smaller interlayer site, whereas K^+ (1.64 Å) is equally parti-tioned between biotite and muscovite. In contrast, Rb^+ (1.72 Å) and Cs^+ (1.88 Å) which are larger than K^+, favour the more open structure of biotite. In octahedral sites, distribution coef-ficients exhibit the sequence Cr^{3+} (0.615 Å) > V^{3+} (0.64 Å) > Sc^{3+} (0.745 Å) for 3+ cations, implying that biotite has the smaller optimum ionic radius for 3+ cations in octahedral sites (Fig. 4b). This is consistent with the smaller mean octahedral metal-oxygen bond length of the M1-M2 site of 1M biotite (2.093 ± 0.027 Å) compared to the M2 site of 2M1 muscovite (2.236 ± 0.021 Å) (Bailey, 1984). We can also infer that octahedral Fe^{3+} is probably slightly favoured in muscovite over biotite on the basis of the ionic radius argument (Fig. 4). For the distribution of divalent transition elements in the VI-sites, it is difficult to evaluate the effects of ionic radius or crystal-field stabilization energy because of the high analytical errors involved in the determination of distribution coefficients for Ni, Cu and Zn.

7.2. Compositional Effects

Li^+ contents of biotite correlate positively with $\Sigma(Al^{IV}+Al^{VI})$ contents of biotite (Fig. 5a). There is a similar, but less evident, relationship between Li^+ and $\Sigma(Al^{IV}+Al^{VI})$ of muscovite (Fig. 5g). The Li contents of biotite and musco-vite also show weak negative correlations with $\Sigma(Fe^{TOT}+Mg)$ contents (not shown), indicating that the main atomic substitu-tion in the micas is $Li_3Al_{-1}\square_{-2}$ in octahedral sites with $Li_2(Fe, Mg)_{-1}\square_{-1}$ being subordinate. The incorporation of Cr, V, and Sc into biotite is controlled by the content of Al^{TOT}, with the slope and its sign depending on ionic radius (Fig. 5b,c,d). Cr shows a stronger positive correlation with Al^{TOT} of biotite, than V. On the other hand, Sc shows a negative corre-lation with Al^{TOT}, indicating that the presence of Al does not promote the incorporation of Sc into the biotite structure. Such correlations, however, are not observed in coexisting musco-vite, because of the relatively small variations of Al^{TOT}. The concentrations of Rb^+ and Cs^+ in biotite show negative cor-relations with K^+, suggesting that the incorporation of the

smaller K^+ cations reduces the optimum ionic radius of the interlayer sites (Figs. 5e,f). A positive correlation between the Co content and $\Sigma(Fe^{TOT} + Mg)$ in muscovite (Fig. 5h) indi-cates that Co incorporation is facilitated by higher contents of the larger Fe^{2+} and Mg^{2+} cations replacing Al^{VI}. Increased amounts of phengite components in muscovite are expected to produce a larger XII-site, due to a smaller tetrahedral rotation angle (α) being required for articulation of the IV and VI-sheets (Harlow, 1995; Guidotti and Sassi, 1998b). Indeed, Volfinger (1974) found that Mg in VI-sites correlated positively with the replacement of K^+ by Rb^+ and Cs^+. However, Rb, Sr, and Cs contents of our muscovites show negative correlations with $\Sigma(Fe^{TOT}+Mg)$, which more likely controls the substitution of these elements rather than Mg^{2+} alone. Thus, the relationships between $\Sigma(Fe^{TOT} + Mg)$ and the contents of Rb, Sr, and Cs in muscovite cannot be attributed to the expansion of interlayer sites by the phengite substitution in muscovite. Instead, it may reflect pressure dependence, because $\Sigma(Fe^{TOT}+Mg)$ in musco-vite increases strongly as a function of pressure (Guidotti and Sassi, 1998b). Substitution of Sr^{2+} and Ba^{2+} into XII-sites of micas must involve a coupled substitution or vacancies to maintain charge balance, but our data do not allow us to identify the mechanism.

Compositional effects on trace element partitioning are evi-dent if solid solution is not ideal and there are interactions between the constituent molecules, so that the excess chemical potentials of these molecules contribute to the equilibrium constant in Eqn. (4). In examining compositional dependence, molar proportions, rather than weight proportions, are used. In general, biotite favours divalent transition elements in VI-sites due to the higher abundance of appropriately sized sites com-pared to coexisting muscovite (Dahl et al., 1993). Based on the same argument, strong affinities of V^{3+} and Sc^{3+} for musco-vite can be explained by appropriate sites for these elements in muscovite.

D_{Li}^* and D_{Sc}^* show negative dependence on Al^{VI} contents of biotite with two different trends depending on metamorphic grade (Figs. 6a,b). The possibility of an effect due to the difference in Al-saturation level between the two groups can be ruled out because sample 88-58, which is the only Al-under-saturated sample from high-T group, shows the same trend as other high-T samples with respect to the distribution of Li and Sc. The reason for the high distribution coefficient of Li in sample 88-32, which belongs to low-T group, is not known. Figure 6c shows that the distribution of Rb between biotite and muscovite is governed by the $\Sigma(Fe^{TOT} + Mg^{2+})$ content of muscovite. Sr and Ba distributions between biotite and musco-vite are strongly controlled both by metamorphic grade and the K contents of biotite (Fig. 6d,e). Figure 6 also shows that the distributions of Li, Sc, Sr and Ba are dependent both on major element composition and metamorphic temperature, making the separation of the two competing factors difficult.

7.3. Temperature Effects

The equilibrium constant K_D in Eqn. (4) should vary with T according to the relation

$$LnK_D = -\frac{\Delta H^o}{RT} + \frac{\Delta S^o}{R} \qquad (8)$$

if the constant K_D is solely determined by $\Delta G^\circ_{exchange}$ of a reaction such as (1). To evaluate thermal effects, D^*_i values for Li, Sc, V, Sr, Ba and Zr are plotted against metamorphic temperature estimated using the garnet-biotite geothermometer (Fig. 7 a–f). Positive correlations between D^*_i and T are seen for Li, Sc, V, Sr and Ba, whereas a negative correlation exists for Zr. D^*_i values for Sc, V, Sr, Cs and Ba have a tendency toward equal partitioning as temperature increases (Fig. 7), as predicted from fundamental thermodynamic considerations. However, all of these trace element partitionings except for V are also controlled by major element compositions. Recall that V concentrations in biotite show the least major element compositional effects among the 3+ cations in VI-sites (Fig. 5c).

Despite the occurrence of Zr^{4+} in biotite and muscovite at trace levels, the chemical potential of Zr is buffered by phase relations with zircon in the rocks. Thus, at equilibrium, partitioning of Zr may reveal changes in P-T. Zr is preferentially incorporated into muscovite over the temperature range of the studied samples (450 to 650°C), resulting in a four-fold decrease in the distribution coefficients (Fig. 7f). Major element compositions are not correlated with the distribution of Zr between biotite and muscovite.

The ratio of D^*_{Cs}/D^*_{Rb} shows good correlation with metamorphic temperature (Fig. 7g). This may be explained by the relationship between the elasticity of interlayer sites and temperature, as shown in Figures 3 and 4. In this scenario, the distribution line for 1+ cations in XII-sites would rotate clockwise around an axis at K^+ as the temperature increases, to approach equal partitioning, resulting in the decrease of D^*_{Cs}/D^*_{Rb} ratios. Elements whose ionic radii are close to the optimum ionic radii for specific sites in the micas do not show significant variation in distribution coefficients with temperature. In addition, as mentioned earlier, D^*_i ratios are also controlled by the phengite contents of muscovite which are correlated with pressure.

Among the trace elements showing thermal dependence, distributions of V and Zr show significant thermal effects with no major element compositional effects. However, for the distribution of Li, Sc, Sr and Ba between biotite and muscovite, it is difficult to separate thermal dependence from major element compositional and structural effects, because X_{Mg} ratios of both biotite and muscovite are dependent on metamorphic temperature, which in turn affects the structure of interlayer sites of micas.

8. CONCLUSIONS

The systematic distribution of trace elements in coexisting biotite and muscovite indicates that equilibrium was achieved between these minerals in the analyzed metamorphic rocks. Distribution behaviour between biotite and muscovite for many elements is compatible with lattice strain theory, especially in interlayer sites of micas. Unfortunately, none of the trace elements investigated promises simply applicable alternative geothermometers for the metamorphic environment. The thermal dependences derived here for Li, Sc, Sr and Ba partitioning between biotite and muscovite are not strong enough, and it was not possible to separate them from major element compositional and structural effects. However, the trace element partitioning data for V and Zr may be used to cross-check con-

ventional geothermometers for samples from a similar range of P-T and bulk composition, especially when conventional geothermometers suffer from retrograde resetting and/or high Fe^{3+} contents. The ranges and dependences of distribution coefficients on major element compositions established here, for quartzofeldspathic and metapelitic rocks from upper greenschist to upper amphibolite facies, also provide important constraints on the values that can be used in modeling trace element zoning of garnet, because biotite and muscovite participate in many prograde metamorphic reactions.

REFERENCES

Bailey S. W. (1984) Crystal chemistry of the true micas. In *Micas* (ed. S. W. Bailey). *Rev. Min.* Vol. 13. Chap. 2, pp. 13–57.

Bea F., Cámara F., Soler J. M. F., Pugnaire M. T. G., Pereira M. D., and Stroh A. (1993) Trace element determination in minerals: Analyses of concentrates versus laser ablation techniques—Case study: Biotites from granitic rocks. *Eur. Winter Conf. Plasma Spectrom.* p. **40.**

Bea F., Montero P., Garut G., and Zacharini F. (1997) Pressure-dependence of rare earth element distribution in amphibolite and granulite-grade garnets. A LA-ICP-MS study. *Geostandards Newslett.* **21,** 253–270.

Beattie P. (1994) What determines the values of mineral/melt partition coefficients? *Mineral. Mag.* **58A,** 63–64.

Beattie P., Drake M., Jones J., Leeman W., Longhi J., McKay G., Nielsen R., Palme H., Shaw D., Takahashi E., and Watson B. (1993) Terminology for trace-element partitioning. *Geochim. Cosmochim. Acta* **57,** 1605–1606.

Berman R. G. (1991) Thermobarometry using multi-equilibrium calculations: A new technique, with petrological applications. *Can. Mineral.* **29,** 833–855.

Blundy J. D. and Wood B. J. (1991) Crystal-chemical controls on the partitioning of Sr and Ba between plagioclase feldspar, silicate melts, and hydrothermal solutions. *Geochim. Cosmochim. Acta* **55,** 193–209.

Blundy J. and Wood B. (1994) Prediction of crystal-melt partition coefficients from elastic moduli. *Nature* **372,** 452–454.

Brenan J. M., Shaw H. F., Ryerson F. J., and Phinney D. L. (1995) Mineral-aqueous fluid partitioning of trace elements at 900°C and 2.0 GPa: Constraints on the trace element chemistry of mantle and deep crustal fluids. *Geochim. Cosmochim. Acta* **59,** 3331–3350.

Brown D., Rivers T., and Calon T. (1992) A structural analysis of a metamorphic fold-thrust belt, northeast Gagnon terrane, Grenville province. *Can. J. Earth Sci.* **29,** 1915–1927.

Butler B. C. M. (1967) Chemical study of minerals from the Moine schists of the Ardnamurchan area, Argyllshire, Scotland. *J. Petrol.* **8,** 233–267.

Connelly J. N., van Gool J., Rivers T., and James D. T. (1996) Field guide to the geology of the Grenville Province of western Labrador. Pre-conference field excursion. Proterozoic Evolution in the North Atlantic Realm, COPENA-ECSOOT-IBTA Conference, Goose Bay, Labrador, July 29–August 2, 1996, Field excursion guide No. 1.

Dahl P. S., Wehn D. C., and Feldmann S. G. (1993) The systematics of trace-element partitioning between coexisting muscovite and biotite in metamorphic rocks from the Black Hills, South Dakota, USA. *Geochim. Cosmochim. Acta* **57,** 2487–2505.

Domanik K. J., Hervig R. L., and Peacock S. M. (1993) Beryllium and boron in subduction zone minerals: An ion microprobe study. *Geochim. Cosmochim. Acta* **57,** 4997–5010.

Dutrow B. L., Holdaway M. J., and Hinton R. W. (1986) Lithium in staurolite and its petrologic significance. *Contrib. Mineral. Petrol.* **94,** 496–506.

Govindaraju K. (1994) 1994 compilation of working values and sample description for 383 geostandards. *Geostandards Newslett.* **18,** p. 158.

Guidotti C. V. and Sassi F. P. (1998a) Miscellaneous isomorphous substitutions in Na-K white micas: A review, with special emphasis to metamorphic micas. *Rend. Fis. Acc. Lincei.* **9,** 57–78.

Guidotti C. V. and Sassi F. P. (1998b) Petrogenetic significance of Na-K white mica mineralogy: Recent advances for metamorphic rocks. *Eur. J. Min.* **10,** 815–854.

Haack U., Heinrichs H., Boneb, M., and Schneider A. (1984) Loss of metals from pelites during regional metamorphism. *Contrib. Mineral. Petrol.* **85,** 116–132.

Harlow G. E. (1995) Crystal chemistry of barian enrichment in micas from metasomatized inclusions in serpentinite, Motagua Fault Zone, Guatemala. *Eur. J. Mineral.* **7,** 775–789.

Heinrich W., Andrehs G., and Franz G. (1997) Monazite-xenotime miscibility gap thermometry; 1. An empirical calibration. *J. Metamorphic Geol.* **15,** 3–16.

Hervig R. L. and Peacock S. M. (1989) Water and trace elements in coexisting muscovite and biotite from metamorphic rocks. *EOS* **70,** 490 (abstr.).

Hickmott D. D. and Spear F. S. (1992) Major and trace-element zoning in garnets from calcareous pelites in the NW Shelburne Falls quadrangle, Massachusetts: Garnet growth histories in retrograded rocks. *J. Petrol.* **33,** 965–1005.

Hickmott D. D., Shimizu N., Spear F. S., and Selverstone J. (1987) Trace-element zoning in a metamorphic garnet. *Geology* **15,** 573–576.

Hodges K. V. and Crowley P. D. (1985) Error estimation and empirical geothermobarometry for pelitic systems. *Amer. Mineral.* **70,** 702–709.

Hoinkes G. (1986) Effect of grossular-content in garnet on the partitioning of Fe and Mg between garnet and biotite. *Contrib. Mineral. Petrol.* **92,** 393–399.

Holdaway, M. J., Mukhopadhyay B., Dyar M. D., Guidotti C. V., and Dutrow B. L. (1997) Garnet-biotite geothermometry revised; new Margules parameters and a natural specimen data set from Maine. *Amer. Mineral.* **82,** 582–595.

Iiyama J. T. (1979) Trace element distribution in rock-forming silicates. The alkali and alkaline earths: Origin and distribution of the elements. *Physics Chem. Earth* **II,** 161–174.

Jackson S. E., Longerich H. P. Dunning G. R., and Fryer B. J. (1992) The application of laser-ablation microprobe-inductively coupled plasma-mass spectrometry (LAM-ICP-MS) to in situ trace-element determinations in minerals. *Can. Mineral.* **30,** 1049–1064.

Jenner G. A., Foley S. F., Jackson S. E., Green T. H., Fryer B. J., and Longerich H. P. (1994) Determination of partition coefficients for trace elements in high pressure-temperature experimental run products by laser ablation microprobe-inductively coupled plasma-mass spectrometry (LAM-ICP-MS). *Geochim. Cosmochim. Acta* **58,** 5099–5103.

Jensen B. B. (1973) Patterns of trace element partitioning. *Geochim. Cosmochim. Acta* **37,** 2227–2242.

Johnson C. A. (1994) Partitioning of zinc among common ferromagnesian minerals and implications for hydrothermal mobilization. *Can. Mineral.* **32,** 121–132.

Kretz R. (1961) Some applications of thermodynamics to coexisting minerals of variable composition. Examples: orthopyroxene-clinopyroxene and orthopyroxene-garnet. *J. Geol.* **69,** 361–387.

Kretz R. (1983) Symbols for rock-forming minerals. *Am. Mineral.* **68,** 277–279.

Kretz R., Campbell J. L., Hoffman E. L., Hartree R., and Teesdale W. J. (1999) Approaches to equilibrium in the distribution of trace elements among the principal minerals in a high-grade metamorphic terrane. *J. Metamorphic Geol.* **17,** 41–59.

LaTourrette T, Hervig R. L., and Holloway J. R. (1995) Trace element partitioning between amphibole, phlogopite, and basanite melt. *Earth. Planet. Sci. Lett.* **135,** 13–30.

Longerich H. P., Jackson S. E., and Günther D. (1996) Laser ablation inductively coupled plasma mass spectrometric transient signal data acquisition and analyte concentration calculation. *J. An. At. Spectr.* **11,** 899–904.

Matsui Y., Onuma N., Nagasawa H., Higuchi H., and Banno S. (1977) Crystal structure control in trace element partition between crystal and magma. *Bull. Soc. Fr. Mineral. Cristallogr.* **100,** 315–324.

Michael P. (1988) Partition coefficients for rare earth elements in mafic minerals of high silica rhyolites: The importance of accessory mineral inclusions. *Geochim. Cosmochim. Acta* **52,** 275–282.

Möller P. (1988) The dependence of partition coefficients on differences of ionic volumes in crystal-melt systems. *Contrib. Mineral. Petrol.* **99,** 62–69.

Moorbath S., Bell K., Leake B. E., and McKerrow W. S. (1968) Geochronological studies in Connemara and Murrisk, Western Ireland. In *Radiometric Dating for Geologists* (eds. E. I. Hamilton and R. M. Farquhar). pp. 259–298. Interscience.

Onuma N., Higuchi H., Wakita H., and Nagasawa H. (1968) Trace element partition between two pyroxenes and the host lava. *Earth Planet. Sci. Lett.* **5,** 47–51.

Rivers T. (1983a) The northern margin of the Grenville Province in western Labrador—Anatomy of an ancient orogenic front. *Precamb. Res.* **22,** 41–73.

Rivers T. (1983b) Progressive metamorphism of pelitic and quartzofeldspathic rocks in the Grenville Province of western Labrador—tectonic implications of bathozone 6 assemblages. *Can J. Earth. Sci.* **20,** 1791–1804.

Rivers T., van Gool J. A. M., and Connelly J. N. (1993) Contrasting tectonic styles in the northern Grenville province: Implications for the dynamics of orogenic fronts. *Geology* **21,** 1127–1130.

Schwarz S. H. (1998) Structural, metamorphic and tectonic studies in central Gagnon terrane, Grenville Province. M. Sc. Thesis, Memorial University of Newfoundland.

Shannon R. D. (1976) Revised effective ionic radii and systematic studies of interatomic distances in halides and chalcogenides. *Acta. Cyst.* **A32,** 751–767.

Shearer C. K., Papike J. J., Simon S. B., and Laul J. C. (1986) Pegmatite-wallrock interaction, Black Hills, South Dakota: Interaction between pegmatite-derived fluids and quartz-micas schist wallrock. *Am. Mineral.* **71,** 518–539.

Taylor R. P., Jackson S. E., Longerich H. P., and Webster J. D. (1997) In situ trace-element analysis of individual silicate melt inclusions by laser ablation microprobe-inductively coupled plasma-mass spectrometry (LAM-ICP-MS). *Geochim. Cosmochim. Acta* **61,** 2559–2567.

van Gool J. A. M. (1992) The thermotectonic development of the Grenville front fold-and-thrust belt in southwestern Labrador. Ph. D. thesis, Memorial University of Newfoundland.

Volfinger M. (1974) Effet de la composition des micas trioctaédriques sur les distributions de Rb et Cs à l'état de traces. *Earth Planet. Sci. Lett.* **24,** 299–304.

Volfinger M. (1976) Effet de la température sur les distributions de Na, Rb et Cs entre la sanidine, la muscovite, la phlogopite et une solution hydrothermale sous une pression de 1 kbar. *Geochim. Cosmochim. Acta* **40,** 267–282.

Volfinger M. and Robert J. L. (1980) Structural control of the distribution of trace elements between silicates and hydrothermal solutions. *Geochim. Cosmochim. Acta* **44,** 1455–1461.

Williams M. L. and Grambling J. A. (1990) Manganese, ferric iron and the equilibrium between garnet and biotite. *Am. Mineral.* **75,** 886–908.

Yang P., Rivers T., and Jackson S. (1999) Crystal-chemical and thermal controls on trace-element partitioning between coexisting garnet and biotite in metamorphic rocks from western Labrador. *Can. Mineral.* **37,** 443–468.

Zen E-an (1963) Components, phases and criteria of chemical equilibrium in rocks. *Am. J. Sci.* **261,** 929–942.